European Journal of Mechanics A/Solids 53 (2015) 311–328

Contents lists available at ScienceDirect

European Journal of Mechanics A/Solids

journal homepage: www.elsevier.com/locate/ejmsol

Computational Piezo-Grains (CPGs) for a highly-efficient micromechanical modeling of heterogeneous piezoelectric–piezomagnetic composites

Peter L. Bishay [a, *], Satya N. Atluri [b]

[a] College of Engineering and Computer Science, California State University, Northridge, CA, USA
[b] Center for Aerospace Research and Education (CARE), University of California, Irvine, CA, USA

ARTICLE INFO

Article history:
Received 3 February 2015
Accepted 18 May 2015
Available online 9 June 2015

Keywords:
Lekhnitskii
Micromechanics
Trefftz

ABSTRACT

Influenced by the need for composites with stronger magneto-electric coupling, we present a novel numerical method called "Computational Piezo-Grains" (CPGs) for modeling different types of piezoelectric/piezomagnetic composites in the microscale. The advantage of this method is that the matrix and the inclusion of a grain can be modeled using only one element in a finite element sense. The geometric shapes of these computational grains mimic the shapes of grains in the microscale and each grain may contain an embedded micro-void or micro-inclusion. The material of the matrix or the inclusion in any grain could be elastic with no couplings, piezoelectric, or piezomagnetic; thus allowing for modeling different configurations of piezo-composites. Lekhnitskii formulation is extended to model any of these composites and is used in the development of these computational grains to express the fields in the matrix and the inclusion of each computational grain.

1. Introduction

Natural multiferroic single-phase compounds are rare, and their magnetoelectric (ME) responses are either relatively weak or occur at temperatures too low for practical applications (Cheong and Mostovoy, 2007). In contrast, multiferroic composites, which incorporate ferroelectric and ferri-/ferromagnetic phases, typically yield giant magnetoelectric coupling response above room temperature, which makes them ready for technological applications (Ryu et al., 2002). In such composites, the ME coupling effect is a byproduct property of the composite structure, which is absent in the individual phases. An electric polarization is induced by a weak AC magnetic field oscillating in the presence of a DC bias field (this is called the direct ME effect), and/or a magnetization polarization appears upon applying an electric field (this is called the converse ME effect). When a magnetic field is applied to a composite, the magnetic phase changes its shape magnetostrictively. The strain is then passed along to the piezoelectric phase, resulting in an electric polarization. Thus, the ME effect in these composites is extrinsic, depending on the composite microstructure and coupling interaction across magnetic–piezoelectric interfaces. Microwave devices, magnetic field sensors, magnetically controlled optoelectronic devices, spintronics, ME multiple-state memory elements, heterogeneous read/write memory devices, ME recording heads and electromagnetic pick-ups are among the suggested technological applications of the magnetoelectric composites (Nan et al., 2008). Historical perspectives, status and future of multiferroic magnetoelectric composites are given in a review paper (Nan et al., 2008).

ME composites could have various connectivity schemes, but the common connectivity schemes are 0-3–type particulate composites of piezoelectric and magnetic oxide grains, 2-2–type laminate ceramic composites consisting of piezoelectric and magnetic oxide layers, and 1-3–type fiber composites with fibers of one phase embedded in the matrix of another phase. The effective ME coefficient depends on details of the composite microstructures, i.e., component phase properties, volume fraction, grain shape, phase connectivity, etc.

Remarkable ME effect of particulate multiferroic composites could be achieved theoretically in composites with a high concentration of particulate magnetic phase, which is well dispersed in large grains of piezoelectric phase. However, there are some difficulties in designing such ME particle composites that lower the ME

* Corresponding author.
E-mail address: bishayp@gmail.com (P.L. Bishay).

http://dx.doi.org/10.1016/j.euromechsol.2015.05.009
0997-7538/

coefficients compared to the theoretical values, such as (1) formation of unwanted phases by chemical reaction during the high temperature sintering process, (2) large thermal expansion mismatch between piezoelectric and ferrite phases that leads to the formation of microcracks, (3) porosity that would decrease the ME effect of bulk composite ceramics (Petrov et al., 2007). (4) Formation of percolation paths because of the not-well-dispersed conductive ferrite phase in the piezoelectric phase. This causes the charges developed in the piezoelectric phase to leak through this conductive path and hence the polarization of the composite will be difficult, and the ME properties will be reduced. Actually the volume fraction of the alloy grains in the piezoelectric matrix is limited by the percolation problem (Nan et al., 2003).

For accurate and reliable modeling of these multiferroic composites, simple unit cell models will not be useful because the microstructure could have microcracks, voids and other unwanted phases, and is sensitive to the distribution of the ferrite phases in the piezoelectric matrix. Computational methods that can simulate the whole microstructure with internal details (microcracks, voids, unwanted inclusions, percolation paths) in a direct numerical simulation are required. Modeling domains with defects (holes, inclusions or cracks) using the ordinary finite element method needs mesh refinement around defects in order to achieve acceptable results for the gradients of fields; hence it is very complex, time-consuming, and costly. Thus, special methods should be used to model defects. Trefftz methods were used to model microstructures with defects, using multi-source-point Trefftz method in (Dong and Atluri, 2012a) for plane elasticity, and Trefftz boundary collocation method for plane piezoelectricity macromechanics developed by Sheng et al. (2006), and micromechanics by Bishay et al. (2014a) based on Lekhnitskii formalism. The boundary element method was also used by Xu and Rajapakse (1998) to analyze piezoelectric materials with elliptical holes. Finite elements with elliptical holes, inclusions or cracks in elastic materials were developed by Zhang and Katsube (1997), Piltner (1985), and Wang and Qin (2012). Hybrid-stress elements were also developed by Ghosh and his co-workers (Ghosh 2011). For piezoelectric materials, Wang et al. (2004) developed a hybrid finite element with a hole based on Lekhnitskii formalism, while Cao et al. (2013) developed a hybrid finite element with defects based on the extended Stroh formalism. Computational cells or grains for direct numerical micromechanical simulation (DNMS) of micro/meso structures were developed by Dong and Atluri (2012b, 2012c, 2012d) for heterogeneous and functionally graded isotropic elastic composite and porous materials, and by (Bishay and Atluri, 2014; Bishay et al., 2014b) for composite and porous piezoelectric materials. In these methods, each cell models an entire grain of the material, with elastic/rigid inclusions or voids. Symmetric Galarkin Boundary Element Method (SGBEM) (Dong and Atluri, 2012e; Dong and Atluri, 2013) was used for micromechanical modeling of voids, inclusions and cracks in heterogeneous elastic materials. Polygonal and Polyhedral elements (2D and 3D Voronoi cells) for coupled electro-mechanical problems without defects were developed by (Ghosh, 2011), by Jayabal and Menzel (2011, 2012a, 2012b) based on Pian's hybrid stress formulation (Pian, 1964), and by Bishay and Atluri (2012) based on Radial Basis Functions (RBF). Switching phenomena in ferroelectric materials were also modeled using these elements in (Sze and Sheng, 2005) and (Bishay and Atluri, 2013).

This paper presents an attempt to micromechanically model piezoelectric-piezomagnetic composites using a new type of efficient finite elements named “Computational Piezo-Grains” (CPGs). Each Computational Piezo-Grain (CPG) is composed of a matrix with/without a void or an inclusion. The shape of each grain is an irregular polygon to mimic the shapes of grains in the micro-scale. The material of the matrix and the inclusion could be elastic, piezoelectric or piezomagnetic. Piezomagnetism, a phenomenon observed in some antiferromagnetic crystals, is the linear magneto-mechanical effect analogous to the linear electromechanical effect of piezoelectricity. It is characterized by a linear coupling between the system's magnetic polarization and mechanical strain. Piezomagnetism differs from its related property of magnetostriction; if an applied magnetic field is reversed in direction, the produced strain changes its sign. Additionally, a non-zero piezomagnetic moment can be produced by mechanical strain alone at zero field. This is not true of magnetostriction (Cullity, 1971). Magnetostriction and electrostriction are analogous second-order effects. These higher-order effects can be represented effectively as first-order when variations in the system parameters are small compared to the initial values of the parameters (IEEE Std 319-1990, 1991).

Since the sources of magnetic anisotropy (McCaig, 1977) are different from those of electrical and mechanical anisotropies, in the proposed formulation we allow the magnetic bias direction to be different from the poling direction or the axis normal to the plane of isotropy in transversely isotropic materials. In (Zhai et al., 2004) the direction of the applied magnetizing field on the ferrite particles was made different from the poling direction of the piezoelectric matrix. Actually, in the proposed 2D analysis, any kind of anisotropy in material properties can be considered.

The paper is organized as follows: Section 2 introduces the governing equations for piezo-materials, while Section 3 presents Trefftz-Lekhnitskii formulation for grains with/without elliptical voids/inclusions. Constructing different types of Computational Piezo-Grains using different methods is given in Section 4 and numerical examples are given in Section 5 to verify the formulation and illustrate the effectiveness of CPGs. Summary and conclusions are provided in Section 6.

2. Governing equations for magneto-electro-elastic (MEE) composites

Consider a domain Ω filled with a general magnetoelectroelastic (MEE) material with piezoelectric, piezomagnetic and magneto-electric couplings. On the boundary of the domain, denoted $\partial\Omega$, we can specify mechanical displacements on S_u or tractions on S_t (not both at any point). Similarly we can specify electric potential on S_φ or electric charge per unit area (electric displacement) on S_Q. We can also specify magnetic potential on S_ψ or magnetic flux density (magnetic induction) on S_B. The whole domain Ω can be divided into N regions or grains $\Omega = \sum_{e=1}^{N} \Omega^e$ (where each region may represent a grain in the material). The intersection between the boundary of grain e, denoted $\partial\Omega^e$, and S_u,S_t,S_φ,S_Q,S_ψ and S_B are $S_u^e, S_t^e, S_\varphi^e, S_Q^e, S_\psi^e$ and S_B^e, while the intersection with the boundaries of neighboring grains is denoted S_g^e. The following relations exist for these aforementioned boundaries:

$$\begin{aligned}
&\partial\Omega = S_u \cup S_t = S_\varphi \cup S_Q = S_\psi \cup S_B \\
&S_u \cap S_t = \varnothing; \quad S_\varphi \cap S_Q = \varnothing; \quad S_\psi \cap S_B = \varnothing \\
&S_u^e = S_u \cap \partial\Omega^e; \quad S_t^e = S_t \cap \partial\Omega^e; \quad etc. \\
&\partial\Omega^e = S_u^e \cup S_t^e \cup S_g^e = S_\varphi^e \cup S_Q^e \cup S_g^e = S_\psi^e \cup S_B^e \cup S_g^e
\end{aligned} \tag{1}$$

Each grain domain, Ω^e, may contain a void or an inclusion filling the domain Ω_c^e and has a boundary $\partial\Omega_c^e$ such that $\Omega_c^e \subset \Omega^e$ and $\partial\Omega_c^e \cap \partial\Omega^e = \varnothing$. In this case, the region outside the void/inclusion domain in grain e is called the matrix domain $\Omega_m^e = \Omega^e - \Omega_c^e$. Fig. 1 shows one grain (irregular polygonal region in the 2D case) with an arbitrary void/inclusion. The figure also shows the matrix poling direction (left) and the matrix magnetic bias direction (right), while Fig. 2 shows the inclusion poling and magnetic bias directions in case the inclusion material is piezoelectric or piezomagnetic,

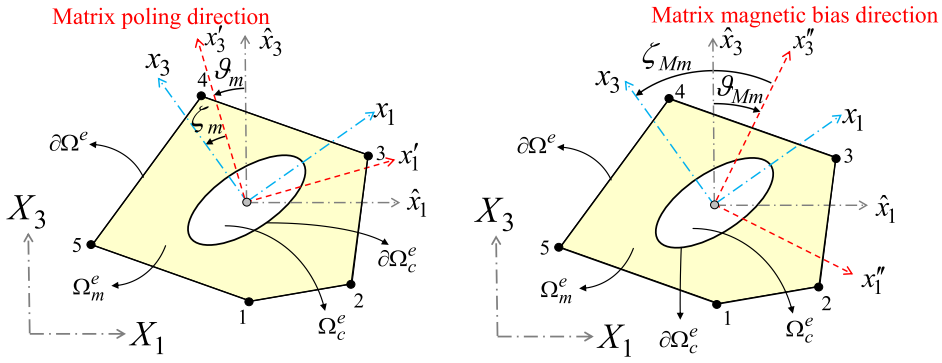

Fig. 1. 2D irregular polygon (grain) with an elliptical void and its local coordinates ($x_1 - x_3$) as well as the global ($X_1 - X_3$), grain local ($\hat{x}_1 - \hat{x}_3$) Cartesian coordinate systems, matrix electric poling direction (x_3'), and matrix magnetic bias direction (x_3'').

respectively. Magnetic bias direction and poling direction are generally allowed to be different. The inclusions and the matrix are assumed to be perfectly bonded, without any sliding on their interfaces.

Adopting matrix and vector notation, and denoting by $\mathbf{u}^\alpha$ (m), $\boldsymbol{\varepsilon}^\alpha$ (m/m) and $\boldsymbol{\sigma}^\alpha$ (Pa or N/m^2), respectively, the mechanical displacement vector, strain and stress tensors written in vector form, by φ^α (V), $\mathbf{E}^\alpha$ (V/m or N/C) and $\mathbf{D}^\alpha$ (C/m^2), respectively, the scalar electric potential, and electric field & electric displacement vectors; and by ψ^α (A or C/s), $\mathbf{H}^\alpha$ (A/m or C/ms) and $\mathbf{B}^\alpha$ (N/Am or Vs/m^2), respectively, the scalar magnetic potential, and magnetic field & magnetic induction (magnetic flux density) vectors respectively, where the superscript $\alpha = m$ or c (for matrix or inclusion), the following equations should be satisfied in the non-conducting matrix and inclusion domains (Ω_m^e andΩ_c^e):

1 Stress equilibrium and the electric and magnetic forms of Gauss's equations:

$$\boldsymbol{\partial}_{\mathbf{u}}^T\boldsymbol{\sigma}^\alpha + \overline{\mathbf{b}}_f^\alpha = 0; \quad \boldsymbol{\sigma}^\alpha = (\boldsymbol{\sigma}^\alpha)^T, \quad \boldsymbol{\partial}_{\mathbf{e}}^T\mathbf{D}^\alpha - \overline{\rho}_f^\alpha = 0, \quad \boldsymbol{\partial}_{\mathbf{e}}^T\mathbf{B}^\alpha = 0 \tag{2}$$

where $\overline{\mathbf{b}}_f^\alpha$ is the body force vector, and $\overline{\rho}_f^\alpha$ is the electric free charge density (which is approximately zero for dielectric and piezoelectric materials). Note that the right hand-side of the third equation in eq. (2) is zero because magnetic free charges do not exist in nature.

2 The strain-displacement (for infinitesimal deformations), electric field-electric potential, and magnetic field-magnetic potential relations, respectively:

$$\boldsymbol{\varepsilon}^\alpha = \boldsymbol{\partial}_{\mathbf{u}}\mathbf{u}^\alpha, \quad \mathbf{E}^\alpha = -\boldsymbol{\partial}_{\mathbf{e}}\varphi^\alpha, \quad \mathbf{H}^\alpha = -\boldsymbol{\partial}_{\mathbf{e}}\psi^\alpha \tag{3}$$

Where for 2D: $\boldsymbol{\partial}_{\mathbf{u}} = \begin{bmatrix} \frac{\partial}{\partial x_1} & 0 & \frac{\partial}{\partial x_3} \\ 0 & \frac{\partial}{\partial x_3} & \frac{\partial}{\partial x_1} \end{bmatrix}^T$ $\boldsymbol{\partial}_{\mathbf{e}} = \begin{bmatrix} \frac{\partial}{\partial x_1} & \frac{\partial}{\partial x_3} \end{bmatrix}^T$

This representation of electric and magnetic fields (eq. (3)), as gradients of electric and magnetic scalar potentials, includes the assumption that Faraday's equation ($\nabla \times \mathbf{E}^\alpha = -\partial\mathbf{B}^\alpha/\partial t = 0$) and Ampere's law with Maxwell's correction ($\nabla \times \mathbf{H}^\alpha = \mathbf{J}^\alpha + \partial\mathbf{D}^\alpha/\partial t = 0$, where $\mathbf{J}^\alpha$ is the electric current density) are satisfied for electrostatics and magnetostatics.

We assume that the materials are electrically non-conducting. Piezoelectric ceramics are good dielectrics so they are normally non-conductors, while piezomagnetic (or magnetostrictive) materials may be insulators (like $NiFe_2O_4$ (Zhai et al., 2004) and $Mn_{1-x}Zn_xFe_2O_4$ (Kamentsev et al., 2006)) and may be conductors (like CoFeV and Terfenol-D (Laletsin et al., 2004)). So when dealing with piezoelectric-piezomagnetic fiber or particle composites subjected to electric loadings, we only consider electrically insulating piezomagnetic materials. Hence we assume, $\mathbf{J}^\alpha = \mathbf{J}_{piezo}^\alpha = \mathbf{J}_{magneto}^\alpha = 0$. Actually without this assumption, the analogy between piezoelectric and piezomagnetic materials breaks down because in this case they are physically different and cannot be modeled with the same set of differential equations (Blackburn et al., 2008).

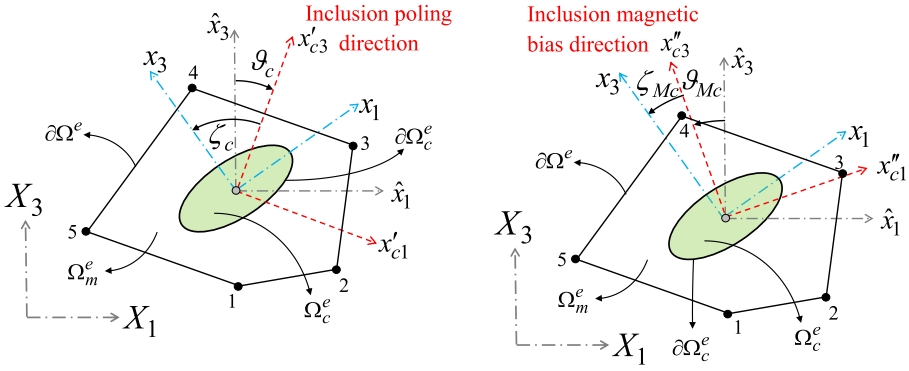

Fig. 2. 2D irregular polygon (grain) with an elliptical inclusion and its local coordinates ($x_1 - x_3$) as well as the global ($X_1 - X_3$), grain local ($\hat{x}_1 - \hat{x}_3$) Cartesian coordinate systems, inclusion electric poling direction (x_{c3}'), and inclusion magnetic bias direction (x_{c3}'').

3 Constitutive laws:

$$\begin{Bmatrix} \boldsymbol{\sigma}^{\alpha} \\ \mathbf{D}^{\alpha} \\ \mathbf{B}^{\alpha} \end{Bmatrix} = \begin{bmatrix} \mathbf{C}^{\alpha} & \mathbf{e}^{\alpha T} & \mathbf{d}^{\alpha T} \\ \mathbf{e}^{\alpha} & -\mathbf{h}^{\alpha} & -\mathbf{n}^{\alpha T} \\ \mathbf{d}^{\alpha} & -\mathbf{n}^{\alpha} & -\mathbf{m}^{\alpha} \end{bmatrix} \begin{Bmatrix} \boldsymbol{\varepsilon}^{\alpha} \\ -\mathbf{E}^{\alpha} \\ -\mathbf{H}^{\alpha} \end{Bmatrix} \quad \text{Or,}$$
$$\begin{Bmatrix} \boldsymbol{\varepsilon}^{\alpha} \\ -\mathbf{E}^{\alpha} \\ -\mathbf{H}^{\alpha} \end{Bmatrix} = \begin{bmatrix} \mathbf{S}^{\alpha} & \mathbf{g}^{\alpha T} & \mathbf{b}^{\alpha T} \\ \mathbf{g}^{\alpha} & -\boldsymbol{\beta}^{\alpha} & -\boldsymbol{\kappa}^{\alpha T} \\ \mathbf{b}^{\alpha} & -\boldsymbol{\kappa}^{\alpha} & -\boldsymbol{\upsilon}^{\alpha} \end{bmatrix} \begin{Bmatrix} \boldsymbol{\sigma}^{\alpha} \\ \mathbf{D}^{\alpha} \\ \mathbf{B}^{\alpha} \end{Bmatrix} \tag{4}$$

where $\mathbf{C}^{\alpha}$ (Pa or N/m^2), $\mathbf{h}^{\alpha}$ (C/Vm), $\mathbf{m}^{\alpha}$ (N/A^2), $\mathbf{S}^{\alpha}$ (m^2/N), $\boldsymbol{\beta}^{\alpha}$ (Vm/C) and $\boldsymbol{\upsilon}^{\alpha}$ (A^2/N) are, respectively, the elastic stiffness, dielectric permittivity, magnetic permeability, elastic compliance, inverse of the permittivity and reluctivity tensors written in matrix form (all are positive definite). $\mathbf{e}^{\alpha}$ (C/m^2) and $\mathbf{g}^{\alpha}$ (m^2/C) are piezoelectric tensors, $\mathbf{d}^{\alpha}$ (N/Am) and $\mathbf{b}^{\alpha}$ (Am/N) are piezomagnetic tensors, and $\mathbf{n}^{\alpha}$ (N/AV) and $\boldsymbol{\kappa}^{\alpha}$ (AV/N) are electromagnetic tensors, all written in matrix form.

If the material of the matrix or the inclusion is not piezoelectric, then the coupling piezoelectric matrices vanish $\mathbf{e}^{\alpha} = \mathbf{g}^{\alpha} = \mathbf{0}$ in eq. (4) and if the material is not piezomagnetic, then $\mathbf{d}^{\alpha} = \mathbf{b}^{\alpha} = \mathbf{0}$. Commercially available monolithic piezoelectric and piezomagnetic materials have very small or no electromagnetic coupling, hence $\mathbf{n}^{\alpha} = \boldsymbol{\kappa}^{\alpha} = \mathbf{0}$.

2.1. Matrix boundary conditions

Mechanical natural (traction) and essential (displacement) boundary conditions:

$$\mathbf{n}_{\boldsymbol{\sigma}}\boldsymbol{\sigma}^{m} = \bar{\mathbf{t}} \quad \text{at } S_t \text{ or } S_t^e, \quad \mathbf{u}^{m} = \bar{\mathbf{u}} \quad \text{at } S_u \text{ or } S_u^e, \tag{5}$$

Electric natural and essential boundary conditions:

$$\mathbf{n}_{\mathbf{e}}\mathbf{D}^{m} = \overline{Q} \quad \text{at } S_Q \text{ or } S_Q^e, \quad \varphi^{m} = \overline{\varphi} \quad \text{at } S_{\varphi} \text{ or } S_{\varphi}^e, \tag{6}$$

Magnetic natural and essential boundary conditions:

$$\mathbf{n}_{\mathbf{e}}\mathbf{B}^{m} = \overline{Q}_M \quad \text{at } S_B \text{ or } S_B^e, \quad \psi^{m} = \overline{\psi} \quad \text{at } S_{\psi} \text{ or } S_{\psi}^e, \tag{7}$$

$$\text{Where for 2D } \mathbf{n}_{\boldsymbol{\sigma}} = \begin{bmatrix} n_1 & 0 & n_3 \\ 0 & n_3 & n_1 \end{bmatrix}, \text{ and } \mathbf{n}_{\mathbf{e}} = [n_1 \;\; n_3], \tag{8}$$

$\bar{\mathbf{t}}$ is the specified boundary traction vector, $\overline{Q}$ is the specified surface charge density (or electric displacement) and $\overline{Q}_M$ is the specified surface magnetic flux density (or magnetic induction). n_1, n_2 and n_3, the three components present in $\mathbf{n}_{\boldsymbol{\sigma}}$ and $\mathbf{n}_{\mathbf{e}}$, are the components of the unit outward normal to the boundaries S_t^e, S_Q^e, or S_B^e respectively. $\bar{\mathbf{u}}$, $\overline{\varphi}$ and $\overline{\psi}$ are the specified mechanical displacement vector, electric and magnetic potentials at the boundaries S_{φ}^e, S_{ψ}^e and S_u^e respectively.

The following conditions should also be satisfied at each intergrain boundaries S_g^e:

1 Mechanical displacement, electric and magnetic potential compatibility conditions:

$$\mathbf{u}^{m+} = \mathbf{u}^{m-}, \quad \varphi^{m+} = \varphi^{m-}, \quad \psi^{m+} = \psi^{m-} \tag{9}$$

2 Mechanical traction, electric and magnetic reciprocity conditions:

$$(\mathbf{n}_{\boldsymbol{\sigma}}\boldsymbol{\sigma}^{m})^{+} + (\mathbf{n}_{\boldsymbol{\sigma}}\boldsymbol{\sigma}^{m})^{-} = 0, \quad (\mathbf{n}_{\mathbf{e}}\mathbf{D}^{m})^{+} + (\mathbf{n}_{\mathbf{e}}\mathbf{D}^{m})^{-} = 0, \quad (\mathbf{n}_{\mathbf{e}}\mathbf{B}^{m})^{+} + (\mathbf{n}_{\mathbf{e}}\mathbf{B}^{m})^{-} = 0 \tag{10}$$

where superscript "+" indicates variables calculated from grain e and directed toward the outward normal direction from its boundaries, while superscript "−" indicates those calculated from the neighboring grains and directed toward grain e.

2.2. Inclusion and impermeable void boundary conditions

We have the following conditions along the inclusion boundary, $\partial\Omega_c^e$:

1 Mechanical displacements, electric and magnetic potential continuity conditions:

$$\mathbf{u}^{m} = \mathbf{u}^{c}, \quad \varphi^{m} = \varphi^{c}, \quad \psi^{m} = \psi^{c} \tag{11}$$

2 Traction reciprocity and continuities of normal electric displacement and magnetic induction:

$$-\mathbf{n}_{\boldsymbol{\sigma}}\boldsymbol{\sigma}^{m} + \mathbf{n}_{\boldsymbol{\sigma}}\boldsymbol{\sigma}^{c} = 0, \quad \mathbf{n}_{\mathbf{e}}\mathbf{D}^{m} = \mathbf{n}_{\mathbf{e}}\mathbf{D}^{c}, \quad \mathbf{n}_{\mathbf{e}}\mathbf{B}^{m} = \mathbf{n}_{\mathbf{e}}\mathbf{B}^{c} \tag{12}$$

The impermeability assumption treats the void as being fully insulated from electromagnetic field (as a result, the electromagnetic field inside the void is always zero). The electric permittivity of piezoelectric materials is three orders of magnitude higher than that of air or vacuum inside the void, while the magnetic permeability of piezomagnetic materials (for example $CoFe_2O_4$) is about two orders of magnitude higher than that of air or vacuum. Hence, the electromagnetic impermeability assumption can be adopted. We then have *traction-free* and *vanishing surface charge density and magnetic flux density* conditions along the void boundary, $\partial\Omega_c^e$:

$$\mathbf{t}^{m} = \mathbf{n}_{\boldsymbol{\sigma}}\boldsymbol{\sigma}^{m} = 0, \quad Q^{m} = \mathbf{n}_{\mathbf{e}}\mathbf{D}^{m} = 0, \quad Q_M^{m} = \mathbf{n}_{\mathbf{e}}\mathbf{B}^{m} = 0 \tag{13}$$

If the magnetic permeability of a porous piezomagnetic material is close to that of air, vacuum or the fluid inside the void, then the void domain should be treated magnetically as an inclusion. This will not be covered in this study.

3. Trefftz-Lekhnitskii formulation

3.1. Basic formulation

The following 2D formulation is suitable for three types of materials: piezoelectric, piezomagnetic and elastic (with no coupling). The formulation can also be used for external domains (matrix), or internal domains (inclusions). As mentioned previously, the magnetic bias direction in the matrix or in the inclusion is allowed to be different from the poling direction or the axis normal to the plane of isotropy in transversely isotropic materials.

Let $(x'_{\alpha 1}, x'_{\alpha 3})$ be the principal material (crystallographic) coordinates in the matrix (α=m) or in the inclusion (α=c), $x'_{\alpha 3}$ be the poling direction (for piezoelectric or dielectric materials) in the matrix or in the inclusion, and $x''_{\alpha 3}$ be the magnetic bias direction in the matrix or in the inclusion (see Figs. 1 and 2). (x_1, x_3) coordinates are obtained by rotating $(x'_{\alpha 1}, x'_{\alpha 3})$ through an anti-clockwise rotationζ_{α}, or by rotating $(x''_{\alpha 1}, x''_{\alpha 3})$ through an anti-clockwise rotation$\zeta_{M\alpha}$, as shown in Fig. 3. In the rest of this section, the

subscript,α, that indicates whether we are talking about the matrix (α=m) or the inclusion (α=c) is omitted for simplicity.

Using Lekhnitskii formalism (Lekhnitskii, 1968, 1981), Xu and Rajapakse (1999) derived the general solution of plane piezoelectricity with respect to (x_1, x_3) coordinate system. Because Lekhnitskii's solution for piezoelectric materials breaks down if there is no coupling between the mechanical and the electrical variables, this study presents this solution in a general form that can be used for coupled as well as uncoupled materials. The formulation is also extended here by including the magnetic variables. Hence, the matrix and the inclusion materials can be piezoelectric, piezomagnetic or elastic (with no couplings) to allow modeling the different types of piezoelectric-piezomagnetic composites in 2D.

The constitutive equation with respect to (x_1, x_3) coordinate system for plane stress and plane strain problems, with stress, electric displacement and magnetic induction as the independent variables of the equations, can be written as:

$$\begin{Bmatrix} \varepsilon_1 \\ \varepsilon_3 \\ \varepsilon_5 \\ E_1 \\ E_3 \\ H_1 \\ H_3 \end{Bmatrix} = \begin{bmatrix} S_{11} & S_{13} & S_{15} & g_{11} & g_{31} & b_{11} & b_{31} \\ S_{13} & S_{33} & S_{35} & g_{13} & g_{33} & b_{13} & b_{33} \\ S_{15} & S_{35} & S_{55} & g_{15} & g_{35} & b_{15} & b_{35} \\ -g_{11} & -g_{13} & -g_{15} & \beta_{11} & \beta_{13} & \kappa_{11} & \kappa_{13} \\ -g_{31} & -g_{33} & -g_{35} & \beta_{13} & \beta_{33} & \kappa_{13} & \kappa_{33} \\ -b_{11} & -b_{13} & -b_{15} & \kappa_{11} & \kappa_{13} & \upsilon_{11} & \upsilon_{13} \\ -b_{31} & -b_{33} & -b_{35} & \kappa_{13} & \kappa_{33} & \upsilon_{13} & \upsilon_{33} \end{bmatrix} \begin{Bmatrix} \sigma_1 \\ \sigma_3 \\ \sigma_5 \\ D_1 \\ D_3 \\ B_1 \\ B_3 \end{Bmatrix} \text{ or}$$

$$\begin{Bmatrix} \boldsymbol{\varepsilon} \\ \mathbf{E} \\ \mathbf{H} \end{Bmatrix} = \begin{bmatrix} \mathbf{S} & \mathbf{g}^T & \mathbf{b}^T \\ -\mathbf{g} & \boldsymbol{\beta} & \boldsymbol{\kappa} \\ -\mathbf{b} & \boldsymbol{\kappa} & \boldsymbol{\upsilon} \end{bmatrix} \begin{Bmatrix} \boldsymbol{\sigma} \\ \mathbf{D} \\ \mathbf{B} \end{Bmatrix} \tag{14}$$

where superscripts of the material matrices in eq. (4) are omitted for simplicity. Tensor transformation rules can be used to express the material properties in (x_1, x_3) coordinate system in terms of those in the crystallographic coordinate system(x_1',x_3'), such as $\mathbf{S}'$,$\mathbf{g}'$,$\boldsymbol{\beta}'$ and $\boldsymbol{\kappa}'$, or in terms of those in the (x_1'',x_3'') coordinate system, such as $\boldsymbol{\upsilon}''$,$\mathbf{b}''$:

$$\begin{aligned} &\mathbf{S} = \mathbf{T}_2^T\mathbf{S}'\mathbf{T}_2, \quad \mathbf{g} = \mathbf{T}_1^T\mathbf{g}'\mathbf{T}_2, \quad \boldsymbol{\beta} = \mathbf{T}_1^T\boldsymbol{\beta}'\mathbf{T}_1, \quad \boldsymbol{\kappa} = \mathbf{T}_1^T\boldsymbol{\kappa}'\mathbf{T}_1 \\ &\mathbf{b} = \mathbf{T}_{\mathbf{M1}}^T\mathbf{b}''\mathbf{T}_{\mathbf{M2}}, \quad \boldsymbol{\upsilon} = \mathbf{T}_{\mathbf{M1}}^T\boldsymbol{\upsilon}''\mathbf{T}_{\mathbf{M1}} \end{aligned} \tag{15}$$

In the above equations,

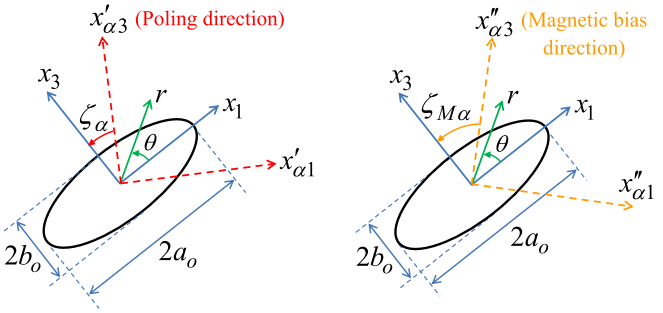

Fig. 3. Elliptical void/inclusion with its local coordinate system ($x_1 - x_3$) as well as the poling direction (left), and magnetic bias direction (right).

$$\mathbf{T}_1 = \begin{bmatrix} \cos\zeta & -\sin\zeta \\ \sin\zeta & \cos\zeta \end{bmatrix} \quad \text{and}$$

$$\mathbf{T}_2 = \begin{bmatrix} \cos^2\zeta & \sin^2\zeta & -2\sin\zeta\cos\zeta \\ \sin^2\zeta & \cos^2\zeta & 2\sin\zeta\cos\zeta \\ \sin\zeta\cos\zeta & -\sin\zeta\cos\zeta & \cos^2\zeta - \sin^2\zeta \end{bmatrix} \tag{16}$$

$\mathbf{T_{M1}}$ and $\mathbf{T_{M2}}$ have the same form of $\mathbf{T_1}$ and $\mathbf{T_2}$ respectively in eq. (16) after replacing ζ by ζ_M. It can be seen that the coefficients $\mathbf{S}$, $\mathbf{g}$,$\boldsymbol{\beta}$,$\boldsymbol{\upsilon}$,$\mathbf{b}$ and $\boldsymbol{\kappa}$ are functions of the anglesζ and ζ_M. Piezoelectric materials have no magneto-mechanical and electromagnetic couplings, so $\mathbf{b} = \boldsymbol{\kappa} = \mathbf{0}$; piezomagnetic materials have no electromechanical and electromagnetic couplings, hence $\mathbf{g} = \boldsymbol{\kappa} = \mathbf{0}$; while elastic dielectric materials have no couplings at all, so $\mathbf{g} = \mathbf{b} = \boldsymbol{\kappa} = \mathbf{0}$.

In the absence of body force and free-charge density ($\overline{\mathbf{b}}_f = 0$, $\overline{\rho_f} = 0$), the balance laws in eq. (2), the strain compatibility ($\partial^2\varepsilon_1/\partial x_3^2 + \partial^2\varepsilon_3/\partial x_1^2 - \partial^2\varepsilon_5/\partial x_1\partial x_3 = 0$), Faraday's ($\partial E_1/\partial x_3 - \partial E_3/\partial x_1 = 0$) and Ampere's ($\partial H_1/\partial x_3 - \partial H_3/\partial x_1 = 0$) equations for 2D electrostatics and magnetostatics as well as the relations in eq. (3) and the constitutive laws in eq. (4) are satisfied using Lekhnitskii's formulation when extended to the case of magneto-electro-elasticity as detailed in Appendix A.

The general expressions for mechanical displacements, electric and magnetic potentials, stress, electric displacement, magnetic induction, strain, electric field and magnetic field components for any type of material can be obtained in terms of the complex potential functions $\omega_k(z_k)$ as:

$$\begin{Bmatrix} u_1 \\ u_3 \\ \varphi \\ \psi \end{Bmatrix} = 2\mathrm{Re}\sum_{k=1}^{4} \begin{Bmatrix} p_k \\ q_k/\mu_k \\ s_k \\ h_k \end{Bmatrix} \omega_k(z_k) \tag{17}$$

$$\begin{aligned} &\begin{Bmatrix} \sigma_1 \\ \sigma_3 \\ \sigma_5 \end{Bmatrix} = 2\mathrm{Re}\sum_{k=1}^{4} \begin{Bmatrix} \gamma_k\mu_k^2 \\ \gamma_k \\ -\gamma_k\mu_k \end{Bmatrix} \omega_k'(z_k), \quad \begin{Bmatrix} \varepsilon_1 \\ \varepsilon_3 \\ \varepsilon_5 \end{Bmatrix} = 2\mathrm{Re}\sum_{k=1}^{4} \begin{Bmatrix} p_k \\ q_k \\ r_k \end{Bmatrix} \omega_k'(z_k), \\ &\begin{Bmatrix} D_1 \\ D_3 \end{Bmatrix} = 2\mathrm{Re}\sum_{k=1}^{4} \begin{Bmatrix} \lambda_k\mu_k \\ -\lambda_k \end{Bmatrix} \omega_k'(z_k), \quad \begin{Bmatrix} E_1 \\ E_3 \end{Bmatrix} = -2\mathrm{Re}\sum_{k=1}^{4} \begin{Bmatrix} s_k \\ t_k \end{Bmatrix} \omega_k'(z_k), \\ &\begin{Bmatrix} B_1 \\ B_3 \end{Bmatrix} = 2\mathrm{Re}\sum_{k=1}^{4} \begin{Bmatrix} \Delta_k\mu_k \\ -\Delta_k \end{Bmatrix} \omega_k'(z_k), \quad \begin{Bmatrix} H_1 \\ H_3 \end{Bmatrix} = -2\mathrm{Re}\sum_{k=1}^{4} \begin{Bmatrix} h_k \\ l_k \end{Bmatrix} \omega_k'(z_k) \end{aligned} \tag{18}$$

where the prime ($'$) denotes derivative with respect to the complex variable $z_k = x_1 + \mu_k x_3$. The other parameters in eqs. 17 and 18 can be found in Appendix A.

3.2. Basic solution set

For an elliptical void/inclusion as shown in Fig. 3, the following conformal mapping can be used to transform the ellipse in z_k-plane into a unit circle in ξ_k-plane (Lekhnitskii, 1981):

$$\xi_k = \frac{z_k \pm \sqrt{z_k^2 - \left(a_o^2 + \mu_k^2 b_o^2\right)}}{a_o - i\mu_k b_o}, \quad k = 1,2,3,4 \tag{19}$$

where a_o and b_o are the half lengths of the void/inclusion axes as shown in Fig. 3, and the sign of the square root ($\pm$) is chosen in such a way that $|\xi_k| \geq 1$. The inverse mapping has the form:

$$z_k = \frac{a_o - i\mu_k b_o}{2}\xi_k + \frac{a_o + i\mu_k b_o}{2}\xi_k^{-1}, \quad k = 1,2,3,4 \tag{20}$$

Using the general solution, the plane magneto-electro-mechanical problem has been reduced to the one of solving the complex potential functions ω_k. For simply connected domains, ω_k can be represented by Taylor series (Domingues et al., 1999), i.e.

$$\omega_k(z_k) = \sum_{n=0}^{\infty}\left(a_k^{(n)} + ib_k^{(n)}\right)z_k^n \quad \text{for } k = 1,2,3,4 \tag{21}$$

For a domain which is exterior to an elliptical void, ω_k can be represented by Laurent series in terms of ξ_k instead of z_k as (Domingues et al., 1999):

$$\omega_k(\xi_k) = \sum_{n=0}^{\infty}\left(a_k^{(n)} + ib_k^{(n)}\right)\xi_k^n + \sum_{n=1}^{\infty}\left(a_k^{(-n)} + ib_k^{(-n)}\right)\xi_k^{-n} \text{ for } k = 1,2,3,4 \tag{22}$$

where $a_k^{(\pm n)}$ and $b_k^{(\pm n)}$ (k = 1,2,3,4 and n = 1,2,3, …) are real coefficients. Along the void/inclusion boundary which is a unit circle in the ξ_k-plane, we have: $|\xi_k| = 1$ or $\xi_k = e^{i\Theta}$ where $\Theta \in [-\pi, \pi]$. Note that $\overline{\xi}_k^n = \xi_k^{-n}$ on the unit circle.

In this case, $\omega_k(z_k)$ and $\omega_k'(z_k)$ are replaced by $\omega_k(\xi_k)$ and $\omega_k'(\xi_k)/z_k'(\xi_k)$ in eqs. (17) and (18), where $z_k' = A - B\xi_k^{-2}$, $A = a_o - i\mu_k b_o/2$; $B = a_o + i\mu_k b_o/2$ and the prime ($'$) now denotes derivative with respect to ξ_k. Hence, in the coming equations, the following will be used:

$$Z_k = \begin{cases} z_k & \text{for simply connected domains} \\ \xi_k & \text{for ellipse} - \text{exterior domains} \end{cases}$$

$$Y_k^{n-1} = \begin{cases} z_k^{n-1} & \text{for simply} - \text{connected domains} \\ \dfrac{\xi_k^{n-1}}{A - B\xi_k^{-2}} & \text{for ellipse} - \text{exterior domains} \end{cases}$$

By substituting ω_k in eq. (21) or (22) into eqs. (17) and (18), the *basic set* of Trefftz functions for magneto-electro-mechanical displacements $\underline{\mathbf{u}} = \{u_1,\ u_3,\ \varphi,\ \psi\}^T$, magneto-electro-mechanical stresses and strains $\underline{\boldsymbol{\sigma}} = \{\sigma_1\ \ \sigma_3\ \ \sigma_5\ \ D_1\ \ D_3\ \ B_1\ \ B_3\}^T$, $\underline{\boldsymbol{\varepsilon}} = \{\varepsilon_1\ \ \varepsilon_3\ \ \varepsilon_5\ \ E_1\ \ E_3\ \ H_1\ \ H_3\}^T$, for interior or exterior domain problems can be obtained as:

$$\underline{\mathbf{u}} = 2\sum_{n=M_s}^{M}\sum_{k=1}^{4}\Big[\left(\mathrm{Re}(\boldsymbol{\mathcal{D}}_k)\mathrm{Re}(Z_k^n) - \mathrm{Im}(\boldsymbol{\mathcal{D}}_k)\mathrm{Im}(Z_k^n)\right)a_k^{(n)} - \left(\mathrm{Re}(\boldsymbol{\mathcal{D}}_k)\mathrm{Im}(Z_k^n) + \mathrm{Im}(\boldsymbol{\mathcal{D}}_k)\mathrm{Re}(Z_k^n)\right)b_k^{(n)}\Big] \tag{23}$$

$$\underline{\boldsymbol{\sigma}} = 2\sum_{n=M_s}^{M}\sum_{k=1}^{4}\Big[\left(\mathrm{Re}(\boldsymbol{\mathcal{G}}_k)\mathrm{Re}\left(nY_k^{n-1}\right) - \mathrm{Im}(\boldsymbol{\mathcal{G}}_k)\mathrm{Im}\left(nY_k^{n-1}\right)\right)a_k^{(n)} - \left(\mathrm{Re}(\boldsymbol{\mathcal{G}}_k)\mathrm{Im}\left(nY_k^{n-1}\right) + \mathrm{Im}(\boldsymbol{\mathcal{G}}_k)\mathrm{Re}\left(nY_k^{n-1}\right)\right)b_k^{(n)}\Big] \tag{24}$$

$$\underline{\boldsymbol{\varepsilon}} = 2\sum_{n=M_s}^{M}\sum_{k=1}^{4}\Big[\left(\mathrm{Re}(\boldsymbol{\mathcal{H}}_k)\mathrm{Re}\left(nY_k^{n-1}\right) - \mathrm{Im}(\boldsymbol{\mathcal{H}}_k)\mathrm{Im}\left(nY_k^{n-1}\right)\right)a_k^{(n)} - \left(\mathrm{Re}(\boldsymbol{\mathcal{H}}_k)\mathrm{Im}\left(nY_k^{n-1}\right) + \mathrm{Im}(\boldsymbol{\mathcal{H}}_k)\mathrm{Re}\left(nY_k^{n-1}\right)\right)b_k^{(n)}\Big] \tag{25}$$

In the above: $\boldsymbol{\mathcal{D}}_k = \{p_k, q_k/\mu_k, s_k, h_k\}^T$, $\boldsymbol{\mathcal{G}}_k = \{\gamma_k\mu_k^2, \gamma_k, -\gamma_k\mu_k, \lambda_k\mu_k, -\lambda_k, \Delta_k\mu_k, -\Delta_k\}^T$,

$\boldsymbol{\mathcal{H}}_k = \{p_k, q_k, r_k, -s_k, -t_k, -h_k, -l_k\}^T$

and the upper limit of n (the maximum order of Z_k used in Trefftz functions) is taken to be M for numerical implementation, while the lower limit M_s is taken as:

$$M_s = \begin{cases} 0 & \text{for interior domains} \\ -M & \text{for exterior domains} \end{cases} \tag{26}$$

For interior/exterior solutions, when n is increased by one, eight/sixteen Trefftz functions with their corresponding undetermined real coefficients $\{a_1^{(\pm n)}, b_1^{(\pm n)}, a_2^{(\pm n)}, b_2^{(\pm n)}, a_3^{(\pm n)}, b_3^{(\pm n)}, a_4^{(\pm n)}, b_4^{(\pm n)}\}$ are added to the solution. So the number of Trefftz functions m_T (or the number of undetermined real coefficients) is:

$$m_T = \begin{cases} 8(M+1) & \text{for interior domain solution} \\ 8(2M+1) & \text{for exterior domain solution} \end{cases} \tag{27}$$

Note that when $n = 0$, the associated eight Trefftz functions correspond to rigid-body and constant potentials modes with vanishing stress, strain, electric displacement, electric field, magnetic induction & magnetic field: $\underline{\boldsymbol{\sigma}} = 0$, $\underline{\boldsymbol{\varepsilon}} = 0, \underline{\mathbf{u}} = 2\sum_{k=1}^{4}[\mathrm{Re}(\boldsymbol{\mathcal{D}}_k)a_k^{(0)} - \mathrm{Im}(\boldsymbol{\mathcal{D}}_k)b_k^{(0)}]$.

Generally, it is impossible to find a closed form solution for $\omega_k(Z_k)$ for arbitrary boundary conditions. For the case of electromagnetically impermeable elliptical voids, a special solution set can be found as presented in the next subsection.

3.3. A special solution set for an impermeable elliptical void

The Trefftz special solution set accounts for the homogeneous boundary conditions of voids, cracks etc. Wang et al. (2004) constructed a special solution set of Trefftz functions for electrically impermeable elliptical voids with axes parallel/perpendicular to poling direction. Sheng et al. (2006) extended this to the case of arbitrarily oriented electrically impermeable elliptical voids. Here we extend this special solution set to the case of electromagnetically impermeable elliptical voids.

For *traction-free* and *vanishing normal electric displacement and magnetic induction* boundary conditions along the void surface, the following conditions should be satisfied:

$$\mathrm{Re}\sum_{k=1}^{4}\gamma_k\omega_k(\xi_k) = 0, \quad \mathrm{Re}\sum_{k=1}^{4}\gamma_k\mu_k\omega_k(\xi_k) = 0,$$
$$\mathrm{Re}\sum_{k=1}^{4}\lambda_k\omega_k(\xi_k) = 0, \quad \mathrm{Re}\sum_{k=1}^{4}\Delta_k\omega_k(\xi_k) = 0 \quad \text{for} \quad |\xi_k| = 1 \tag{28}$$

which can be written in matrix form as,

$$\begin{Bmatrix} \overline{\omega}_1 \\ \overline{\omega}_2 \\ \overline{\omega}_3 \\ \overline{\omega}_4 \end{Bmatrix} = \begin{bmatrix} E_{11} & E_{12} & E_{13} & E_{14} \\ E_{21} & E_{22} & E_{23} & E_{24} \\ E_{31} & E_{32} & E_{33} & E_{34} \\ E_{41} & E_{42} & E_{43} & E_{44} \end{bmatrix} \begin{Bmatrix} \omega_1 \\ \omega_2 \\ \omega_3 \\ \omega_4 \end{Bmatrix} \quad \text{for} \quad |\xi_k| = 1 \tag{29}$$

Where the overbar here indicates complex conjugate and

$$\begin{bmatrix} E_{11} & E_{12} & E_{13} & E_{14} \\ E_{21} & E_{22} & E_{23} & E_{24} \\ E_{31} & E_{32} & E_{33} & E_{34} \\ E_{41} & E_{42} & E_{43} & E_{44} \end{bmatrix} = - \begin{bmatrix} \gamma_1 & \gamma_2 & \gamma_3 & \gamma_4 \\ \gamma_1\overline{\mu}_1 & \gamma_2\overline{\mu}_2 & \gamma_3\overline{\mu}_3 & \gamma_4\overline{\mu}_4 \\ \overline{\lambda}_1 & \overline{\lambda}_2 & \overline{\lambda}_3 & \overline{\lambda}_4 \\ \overline{\Delta}_1 & \overline{\Delta}_2 & \overline{\Delta}_3 & \overline{\Delta}_4 \end{bmatrix}^{-1} \begin{bmatrix} \gamma_1 & \gamma_2 & \gamma_3 & \gamma_4 \\ \gamma_1\mu_1 & \gamma_2\mu_2 & \gamma_3\mu_3 & \gamma_4\mu_4 \\ \lambda_1 & \lambda_2 & \lambda_3 & \lambda_4 \\ \Delta_1 & \Delta_2 & \Delta_3 & \Delta_4 \end{bmatrix}$$

Assuming $\omega_k(\xi_k)$ in a form similar to that of eq. (22) and substituting it into eq. (29) yields eight constraint equations on the sixteen real coefficients $a_k^{(n)}, b_k^{(n)}, a_k^{(-n)}$ and $b_k^{(-n)}$ (k=1,2,3,4). By expressing $a_k^{(-n)}$ and $b_k^{(-n)}$ in terms of $a_k^{(n)}$ and $b_k^{(n)}$, we get:

$$\begin{aligned} a_k^{(-n)} &= \sum_{j=1}^{4}\left[\mathrm{Re}\left(E_{kj}\right)a_j^{(n)} - \mathrm{Im}\left(E_{kj}\right)b_j^{(n)}\right], \\ b_k^{(-n)} &= -\sum_{j=1}^{4}\left[\mathrm{Im}\left(E_{kj}\right)a_j^{(n)} + \mathrm{Re}\left(E_{kj}\right)b_j^{(n)}\right] \end{aligned} \tag{30}$$

So the number of Trefftz functions m_T (or the number of undetermined real coefficients) is reduced to $m_T = 8(M+1)$. Substituting eq. (30) into eqs. 23–25 yields the following *special set* of Trefftz functions:

$$\begin{aligned} \underline{\mathbf{u}}_{void} &= \sum_{n=0}^{\infty}\sum_{k=1}^{4}\left[\Phi_{a_k}^{(n)}a_k^{(n)} + \Phi_{b_k}^{(n)}b_k^{(n)}\right], \\ \underline{\boldsymbol{\sigma}}_{void} &= \sum_{n=0}^{\infty}\sum_{k=1}^{4}\left[\Psi_{a_k}^{(n)}a_k^{(n)} + \Psi_{b_k}^{(n)}b_k^{(n)}\right] \\ \underline{\boldsymbol{\varepsilon}}_{void} &= \sum_{n=0}^{\infty}\sum_{k=1}^{4}\left[\Gamma_{a_k}^{(n)}a_k^{(n)} + \Gamma_{b_k}^{(n)}b_k^{(n)}\right] \end{aligned} \tag{31}$$

where:

$$\begin{aligned} \Phi_{a_k}^{(n)} &= \chi_{a_k}^{(n)} + \sum_{j=1}^{4}\left[\mathrm{Re}\left(E_{jk}\right)\chi_{a_j}^{(-n)} - \mathrm{Im}\left(E_{jk}\right)\chi_{b_j}^{(-n)}\right], \quad \Phi_{b_k}^{(n)} = \chi_{b_k}^{(n)} - \sum_{j=1}^{4}\left[\mathrm{Im}\left(E_{jk}\right)\chi_{a_j}^{(-n)} + \mathrm{Re}\left(E_{jk}\right)\chi_{b_j}^{(-n)}\right] \\ \Psi_{a_k}^{(n)} &= \Sigma_{a_k}^{(n)} + \sum_{j=1}^{4}\left[\mathrm{Re}\left(E_{jk}\right)\Sigma_{a_j}^{(-n)} - \mathrm{Im}\left(E_{jk}\right)\Sigma_{b_j}^{(-n)}\right], \quad \Psi_{b_k}^{(n)} = \Sigma_{b_k}^{(n)} - \sum_{j=1}^{4}\left[\mathrm{Im}\left(E_{jk}\right)\Sigma_{a_j}^{(-n)} + \mathrm{Re}\left(E_{jk}\right)\Sigma_{b_j}^{(-n)}\right] \\ \Gamma_{a_k}^{(n)} &= \Upsilon_{a_k}^{(n)} + \sum_{j=1}^{4}\left[\mathrm{Re}\left(E_{jk}\right)\Upsilon_{a_j}^{(-n)} - \mathrm{Im}\left(E_{jk}\right)\Upsilon_{b_j}^{(-n)}\right], \quad \Gamma_{b_k}^{(n)} = \Upsilon_{b_k}^{(n)} - \sum_{j=1}^{4}\left[\mathrm{Im}\left(E_{jk}\right)\Upsilon_{a_j}^{(-n)} + \mathrm{Re}\left(E_{jk}\right)\Upsilon_{b_j}^{(-n)}\right] \end{aligned} \tag{32}$$

and in (32):

$$\begin{aligned} \chi_{a_k}^{(\pm n)} &= 2\mathrm{Re}(\mathcal{D}_k)\mathrm{Re}\left(\xi_k^{\pm n}\right) - 2\mathrm{Im}(\mathcal{D}_k)\mathrm{Im}\left(\xi_k^{\pm n}\right), \\ \chi_{b_k}^{(\pm n)} &= -2\mathrm{Re}(\mathcal{D}_k)\mathrm{Im}\left(\xi_k^{\pm n}\right) - 2\mathrm{Im}(\mathcal{D}_k)\mathrm{Re}\left(\xi_k^{\pm n}\right), \end{aligned}$$

$$\begin{aligned} \Sigma_{a_k}^{(\pm n)} &= \pm 2n\left[\mathrm{Re}(\mathcal{G}_k)\mathrm{Re}\left(\frac{\xi_k^{\pm n-1}}{z_k'}\right) - \mathrm{Im}(\mathcal{G}_k)\mathrm{Im}\left(\frac{\xi_k^{\pm n-1}}{z_k'}\right)\right], \\ \Sigma_{b_k}^{(\pm n)} &= \mp 2n\left[\mathrm{Re}(\mathcal{G}_k)\mathrm{Im}\left(\frac{\xi_k^{\pm n-1}}{z_k'}\right) + \mathrm{Im}(\mathcal{G}_k)\mathrm{Re}\left(\frac{\xi_k^{\pm n-1}}{z_k'}\right)\right], \end{aligned}$$

$$\begin{aligned} \Upsilon_{a_k}^{(\pm n)} &= \pm 2n\left[\mathrm{Re}(\mathcal{H}_k)\mathrm{Re}\left(\frac{\xi_k^{\pm n-1}}{z_k'}\right) - \mathrm{Im}(\mathcal{H}_k)\mathrm{Im}\left(\frac{\xi_k^{\pm n-1}}{z_k'}\right)\right], \\ \Upsilon_{b_k}^{(\pm n)} &= \mp 2n\left[\mathrm{Re}(\mathcal{H}_k)\mathrm{Im}\left(\frac{\xi_k^{\pm n-1}}{z_k'}\right) + \mathrm{Im}(\mathcal{H}_k)\mathrm{Re}\left(\frac{\xi_k^{\pm n-1}}{z_k'}\right)\right], \end{aligned}$$

All variables should be expressed in the grain's Cartesian local coordinate system ($\widehat{x}_1 - \widehat{x}_3$ is Fig. 1 or Fig. 2), hence tensor transformation rule can be used again to do this rotation by an angle $-(\zeta_\alpha + \vartheta_\alpha)$.

4. Formulation of Computational Piezo-Grains (CPGs) for piezoelectric/piezomagnetic materials with/without voids/inclusions

In this section, Computational Piezo-Grains (CPGs) are developed for the Direct Numerical Simulation (DNS) of the micromechanics of piezoelectric-piezomagnetic composites and porous materials where each computational grain has an arbitrarily polygonal shape, and may or may not include a circular or an arbitrarily oriented elliptical void or inclusion. The advantage of using CPGs is that each CPG may represent a single grain in the material that has its own electric poling and magnetic bias directions. The Dirichlet tessellation used to construct the mesh or the geometric shapes of CPGs resembles the physical configurations of grains in the meso-mechanics, wherein each grain may be surrounded by an arbitrary number of neighboring grains; hence CPGs are expected to show field distributions that cannot be obtained using regular triangular or quadrilateral elements. Lekhnitskii's formalism, presented in the previous section, is employed here due to the relatively explicit nature of the derived Trefftz functions.

The matrix-boundary-primal-fields' continuity and the void/inclusion boundary conditions can be enforced using three methods: boundary variational principle (BVP), collocation (C), or least squares (LS). Accordingly, several types of computational grains can be formulated. For CPGs that include voids, the *special solution set* for electromagnetically impermeable elliptical voids, presented in Section 3.3, can be used alternatively. This results in no need to enforce the void boundary conditions separately, using any of the previously mentioned methods, and makes the resulting

computational grains more efficient for modeling grains with electromagnetically impermeable voids.

Consider a 2D irregular m-sided polygonal grain with/without a void or an inclusion as shown in Fig. 1 (left). We can define linear displacements, electric and magnetic potential fields along each grain boundary in terms of the nodal values of the mechanical displacements $\mathbf{q_u}$, electric potential $\mathbf{q}_\varphi$, and magnetic potential $\mathbf{q}_\psi$, as:

$$\tilde{\mathbf{u}} = \tilde{\mathbf{N}}_\mathbf{u}\mathbf{q}_\mathbf{u}, \quad \tilde{\varphi} = \tilde{\mathbf{N}}_\varphi\mathbf{q}_\varphi, \quad \tilde{\psi} = \tilde{\mathbf{N}}_\psi\mathbf{q}_\psi$$
$$\text{or} \quad \underline{\tilde{\mathbf{u}}} = \begin{Bmatrix} \tilde{\mathbf{u}} \\ \tilde{\varphi} \\ \tilde{\psi} \end{Bmatrix} = \begin{bmatrix} \tilde{\mathbf{N}}_\mathbf{u} & 0 & 0 \\ 0 & \tilde{\mathbf{N}}_\varphi & 0 \\ 0 & 0 & \tilde{\mathbf{N}}_\psi \end{bmatrix} \begin{Bmatrix} \mathbf{q}_\mathbf{u} \\ \mathbf{q}_\varphi \\ \mathbf{q}_\psi \end{Bmatrix} = \tilde{\mathbf{N}}\mathbf{q} \quad \text{at } \partial\Omega^e \tag{33}$$

where $\tilde{\mathbf{N}}_\mathbf{u}$, $\tilde{\mathbf{N}}_\varphi$ and $\tilde{\mathbf{N}}_\psi$ are linear shape functions, $\underline{\tilde{\mathbf{u}}} = \begin{bmatrix} \tilde{u}_1 & \tilde{u}_3 & \tilde{\varphi} & \tilde{\psi} \end{bmatrix}^T$ and $\mathbf{q}^T = \begin{Bmatrix} \mathbf{q}_\mathbf{u}^T & \mathbf{q}_\varphi^T & \mathbf{q}_\psi^T \end{Bmatrix}$.

Fields in the matrix and the inclusion can be written in the form:

$$\begin{Bmatrix} \mathbf{u}^\alpha \\ \varphi^\alpha \\ \psi^\alpha \end{Bmatrix} = \begin{Bmatrix} \mathbf{N}_\mathbf{u}^\alpha \\ \mathbf{N}_\varphi^\alpha \\ \mathbf{N}_\psi^\alpha \end{Bmatrix} \mathbf{c}^\alpha, \quad \begin{Bmatrix} \boldsymbol{\sigma}^\alpha \\ \mathbf{D}^\alpha \\ \mathbf{B}^\alpha \end{Bmatrix} = \begin{Bmatrix} \mathbf{M}_\boldsymbol{\sigma}^\alpha \\ \mathbf{M}_\mathbf{D}^\alpha \\ \mathbf{M}_\mathbf{B}^\alpha \end{Bmatrix} \mathbf{c}^\alpha, \quad \text{in } \Omega^e \tag{34}$$
$$\text{or} \quad \underline{\mathbf{u}}^\alpha = \mathbf{N}^\alpha\mathbf{c}^\alpha, \quad \underline{\boldsymbol{\sigma}}^\alpha = \mathbf{M}^\alpha\mathbf{c}^\alpha, \quad \text{in } \Omega^e$$

where $\mathbf{N}^\alpha$ are the Trefftz functions in the order of M_s,...,0,1,...,M and $\mathbf{c}^\alpha$ denotes the unknown real coefficients ($a_k^{(\pm n)}$, $b_k^{(\pm n)}$, k = 1,2,3,4 and $n = M_s$,...,M) associated with Trefftz functions for the matrix ($\alpha = m$) or the inclusion ($\alpha = c$). If there is no void or inclusion, only the non-negative exponents are used. $\mathbf{N}^\alpha$ and $\mathbf{M}^\alpha$ are taken from eqs. (23) and (24) for interior/exterior fields, satisfying the constitutive law, the strain-displacement, electric field-electric potential, and magnetic field-magnetic potential relationships, and the equilibrium and Maxwell's equations, or from eq. (31) which satisfy the void *stress-free* and *vanishing surface charge and magnetic flux densities* boundary conditions when dealing with electromagnetically impermeable elliptical void.

The tractions, surface electric charge density and surface magnetic flux density on the matrix boundaries are:

$$\mathbf{t}^\alpha = \mathbf{n}_\boldsymbol{\sigma}\boldsymbol{\sigma}^\alpha = \mathbf{n}_\boldsymbol{\sigma}\mathbf{M}_\boldsymbol{\sigma}^\alpha\mathbf{c}^\alpha, \quad Q = \mathbf{n}_\mathbf{e}\mathbf{D}^\alpha = \mathbf{n}_\mathbf{e}\mathbf{M}_\mathbf{D}^\alpha\mathbf{c}^\alpha,$$
$$Q_M^\alpha = \mathbf{n}_\mathbf{e}\mathbf{B}^\alpha = \mathbf{n}_\mathbf{e}\mathbf{M}_\mathbf{B}^\alpha\mathbf{c}^\alpha \quad \text{at } \partial\Omega^e \text{ or } \partial\Omega_c^e,$$
$$\text{or} \quad \underline{\mathbf{t}}^\alpha = \begin{Bmatrix} \mathbf{t}^\alpha \\ Q^\alpha \\ Q_M^\alpha \end{Bmatrix} = \begin{bmatrix} \mathbf{n}_\boldsymbol{\sigma} & 0 & 0 \\ 0 & \mathbf{n}_\mathbf{e} & 0 \\ 0 & 0 & \mathbf{n}_\mathbf{e} \end{bmatrix} \begin{Bmatrix} \boldsymbol{\sigma}^\alpha \\ \mathbf{D}^\alpha \\ \mathbf{B}^\alpha \end{Bmatrix} = \underline{\mathbf{n}}\underline{\boldsymbol{\sigma}}^\alpha = \underline{\mathbf{n}}\mathbf{M}^\alpha\mathbf{c}^\alpha$$
$$\text{at } \partial\Omega^e \text{ or } \partial\Omega_c^e, \tag{35}$$

Now, three steps should be done:

Step one: the matrix interior primal fields should be related to the matrix boundary primal fields. Once the mechanical displacements, and the electric and magnetic potentials are expressed in terms of their nodal values in each grain, their continuities (eq. (9)) are automatically satisfied, and the essential boundary conditions (in eqs. (5) and(6)) can be easily enforced after generating the global system of equations.
Step two: the reciprocity conditions (eq. (10)) as well as the natural boundary conditions (in eqs. (5) and (6)) should be enforced.
Step three: (if a void or an inclusion exists in the grain) the conditions on the void/inclusion boundary should also be satisfied as mentioned in subsection 2.2.

A multi-field boundary variational principle (BVP) can be used to enforce all these three steps. Collocation and least squares methods can also be used to enforce steps one and three, then a primal variational principle (PVP) can be used to enforce step two. For the case of a grain with an electromagnetically impermeable void, the special solution set, presented in Section 3.3, can alternatively be used to satisfy step three. This makes the resulting grains more efficient because there is no need to consider any conditions on the void periphery. However, if the void is pressurized, filled with conducting fluid or if the void is replaced by any type of inclusions, the special solution set cannot be used. When the void/inclusion boundary $\partial\Omega_c^e$ shrinks to zero, the grain is reduced to the case of a grain with no defect.

4.1. CPGs based on multi-field boundary variational principle

A multi-field boundary variational principle whose Euler–Lagrange equations (stationarity conditions) are the natural BCs, the reciprocity conditions, as well as the compatibility between interior and boundary fields can be used to derive the grain equation, with the following scalar functional:

$$\begin{aligned} &\Pi_1(u_i^m, u_i^c, \tilde{u}_i, \varphi^m, \varphi^c, \tilde{\varphi}, \psi^m, \psi^c, \tilde{\psi}) \\ &= \sum_{e=1}^{N} \Bigg\{ - \int_{\partial\Omega^e + \partial\Omega_c^e} \frac{1}{2}(t_i^m u_i^m + Q^m\varphi^m + Q_M^m\psi^m)dS \\ &\quad + \int_{\partial\Omega^e} (t_i^m\tilde{u}_i + Q^m\tilde{\varphi} + Q_M^m\tilde{\psi})dS + \int_{\partial\Omega_c^e} (t_i^m u_i^c + Q^m\varphi^c + Q_M^m\psi^c)dS \\ &\quad + \int_{\partial\Omega_c^e} \frac{1}{2}(t_i^c u_i^c + Q^c\varphi^c + Q_M^c\psi^c)dS - \int_{S_t^e} \bar{t}_i\tilde{u}_i dS \\ &\quad - \int_{S_Q^e} \overline{Q}\tilde{\varphi}dS - \int_{S_B^e} \overline{Q}_M\tilde{\psi}dS \Bigg\} \end{aligned} \tag{36}$$

where $i = 1, 3$ in eq. (36) and the equations to follow. This achieves the three steps simultaneously. In matrix and vector notation, Π_1 can be written as:

$$\begin{aligned} \Pi_1\left(\underline{\mathbf{u}}^m, \underline{\mathbf{u}}^c, \underline{\tilde{\mathbf{u}}}\right) = \sum_{e=1}^{N} \Bigg\{ &- \int_{\partial\Omega^e + \partial\Omega_c^e} \frac{1}{2}\underline{\mathbf{t}}^m \cdot \underline{\mathbf{u}}^m dS + \int_{\partial\Omega^e} \underline{\mathbf{t}}^m \cdot \underline{\tilde{\mathbf{u}}}\, dS \\ &+ \int_{\partial\Omega_c^e} \underline{\mathbf{t}}^m \cdot \underline{\mathbf{u}}^c dS + \int_{\partial\Omega_c^e} \frac{1}{2}\underline{\mathbf{t}}^c \cdot \underline{\mathbf{u}}^c dS - \int_{S_t^e} \bar{\mathbf{t}} \cdot \tilde{\mathbf{u}} dS \\ &- \int_{S_Q^e} \overline{Q}\tilde{\phi}dS - \int_{S_B^e} \overline{Q}_M\tilde{\psi}dS \Bigg\} \end{aligned} \tag{37}$$

$$\Pi_1(\mathbf{c}^m, \mathbf{c}^c, \mathbf{q}) = \sum_{e=1}^{N} \Big\{ -\frac{1}{2}\mathbf{c}^{mT}\mathbf{H}_\mathbf{mm}\mathbf{c}^m + \mathbf{c}^{mT}\mathbf{G}_\mathbf{mq}\mathbf{q} + \mathbf{c}^{mT}\mathbf{G}_\mathbf{mc}\mathbf{c}^c + \frac{1}{2}\mathbf{c}^{cT}\mathbf{H}_\mathbf{cc}\mathbf{c}^c - \mathbf{q}^T\mathbf{Q} \Big\} \tag{38}$$

where

$$\mathbf{H_{mm}} = \int_{\partial\Omega^e+\partial\Omega_c^e} \mathbf{M}^{mT}\underline{\mathbf{n}}^T\mathbf{N}^m dS; \quad \mathbf{G_{mc}} = \int_{\partial\Omega_c^e} \mathbf{M}^{mT}\underline{\mathbf{n}}^T\mathbf{N}^c dS; \quad \mathbf{H_{cc}} = \int_{\partial\Omega_c^e} \mathbf{M}^{cT}\underline{\mathbf{n}}^T\mathbf{N}^c dS;$$
$$\mathbf{G_{mq}} = \int_{\partial\Omega^e} \mathbf{M}^{mT}\underline{\mathbf{n}}^T\tilde{\mathbf{N}} dS; \quad \mathbf{Q}^T = \left[\int_{S_t^e} \bar{\mathbf{t}}^T\tilde{\mathbf{N}}_{\mathbf{u}} dS \quad \int_{S_Q^e} \overline{Q}\tilde{\mathbf{N}}_{\phi} dS \quad \int_{S_B^e} \overline{Q}_M\tilde{\mathbf{N}}_{\psi} dS\right] \tag{39}$$

Setting the variation of Π_1 to zero gives:

$$\begin{aligned}\delta\Pi_1(\delta\mathbf{c}^m,\delta\mathbf{c}^c,\delta\mathbf{q}) = \sum_{e=1}^{N}\Big\{ &-\delta\mathbf{c}^{mT}\mathbf{H_{mm}}\mathbf{c}^m + \delta\mathbf{c}^{mT}\mathbf{G_{mq}}\mathbf{q} + \delta\mathbf{q}^T\mathbf{G}_{\mathbf{mq}}^T\mathbf{c}^m \\ &+ \delta\mathbf{c}^{mT}\mathbf{G_{mc}}\mathbf{c}^c + \delta\mathbf{c}^{cT}\mathbf{G}_{\mathbf{mc}}^T\mathbf{c}^m + \delta\mathbf{c}^{cT}\mathbf{H_{cc}}\mathbf{c}^c \\ &- \delta\mathbf{q}^T\mathbf{Q}\Big\} = \sum_{e=1}^{N}\Big\{\delta\mathbf{q}^T\left(\mathbf{G}_{\mathbf{mq}}^T\mathbf{c}^m - \mathbf{Q}\right) \\ &+ \delta\mathbf{c}^{mT}\left(\mathbf{G_{mq}}\mathbf{q} - \mathbf{H_{mm}}\mathbf{c}^m + \mathbf{G_{mc}}\mathbf{c}^c\right) \\ &+ \delta\mathbf{c}^{cT}\left(\mathbf{G}_{\mathbf{mc}}^T\mathbf{c}^m + \mathbf{H_{cc}}\mathbf{c}^c\right)\Big\} = 0\end{aligned} \tag{40}$$

For arbitrary $\delta\mathbf{c}^{mT}$, $\delta\mathbf{c}^{cT}$ and $\delta\mathbf{q}^T$ we can write:

$$\begin{aligned}&\mathbf{G}_{\mathbf{mq}}^T\mathbf{c}^m - \mathbf{Q} = 0, \quad \mathbf{G_{mq}}\mathbf{q} - \mathbf{H_{mm}}\mathbf{c}^m + \mathbf{G_{mc}}\mathbf{c}^c = 0, \\ &\mathbf{G}_{\mathbf{mc}}^T\mathbf{c}^m + \mathbf{H_{cc}}\mathbf{c}^c = 0\end{aligned} \tag{41}$$

Using the second equation, we can write $\mathbf{c}^m$ in terms of $\mathbf{c}^c$ and $\mathbf{q}$:

$$\mathbf{c}^m = \mathbf{H}_{\mathbf{mm}}^{-1}\mathbf{G_{mq}}\mathbf{q} + \mathbf{H}_{\mathbf{mm}}^{-1}\mathbf{G_{mc}}\mathbf{c}^c \tag{42}$$

Substituting this into the first and third equations gives:

$$\begin{bmatrix}\mathbf{G}_{\mathbf{mq}}^T\mathbf{H}_{\mathbf{mm}}^{-1}\mathbf{G_{mq}} & \mathbf{G}_{\mathbf{mq}}^T\mathbf{H}_{\mathbf{mm}}^{-1}\mathbf{G_{mc}} \\ \mathbf{G}_{\mathbf{mc}}^T\mathbf{H}_{\mathbf{mm}}^{-1}\mathbf{G_{mq}} & \mathbf{G}_{\mathbf{mc}}^T\mathbf{H}_{\mathbf{mm}}^{-1}\mathbf{G_{mc}} + \mathbf{H_{cc}}\end{bmatrix}\begin{Bmatrix}\mathbf{q}\\ \mathbf{c}^c\end{Bmatrix} = \begin{Bmatrix}\mathbf{Q}\\ 0\end{Bmatrix} \tag{43}$$

Static condensation can reduce this to the following finite element equation in terms of $\mathbf{q}$ only:

$$\mathbf{K_{bvp}}\mathbf{q} = \mathbf{Q} \tag{44}$$

where

$$\begin{aligned}\mathbf{K_{bvp}} = \mathbf{G}_{\mathbf{mq}}^T\mathbf{H}_{\mathbf{mm}}^{-1}\mathbf{G_{mq}} + \mathbf{G}_{\mathbf{mq}}^T\mathbf{H}_{\mathbf{mm}}^{-1}\mathbf{G_{mc}}\left(\mathbf{G}_{\mathbf{mc}}^T\mathbf{H}_{\mathbf{mm}}^{-1}\mathbf{G_{mc}} + \mathbf{H_{cc}}\right)^{-1} \\ \times \mathbf{G}_{\mathbf{mc}}^T\mathbf{H}_{\mathbf{mm}}^{-1}\mathbf{G_{mq}}\end{aligned} \tag{45}$$

If the grain contains a void instead of an inclusion, we use a boundary field along the void periphery as:

$$\tilde{\underline{\mathbf{u}}}^c = \tilde{\mathbf{N}}^c\mathbf{c}^c \tag{46}$$

where $\tilde{\mathbf{N}}^c$ can still be taken from eq. (23) but with substituting the material properties of the matrix.

In this case, the functional Π_1 should be modified as follows:

$$\begin{aligned}\Pi_{1v}\left(\underline{\mathbf{u}}^m,\tilde{\underline{\mathbf{u}}},\tilde{\underline{\mathbf{u}}}^c\right) = \sum_{e=1}^{N}\Bigg\{ &-\int_{\partial\Omega^e+\partial\Omega_c^e}\frac{1}{2}\underline{\mathbf{t}}^m\cdot\underline{\mathbf{u}}^m dS + \int_{\partial\Omega^e}\underline{\mathbf{t}}^m\cdot\tilde{\underline{\mathbf{u}}}\, dS \\ &+ \int_{\partial\Omega_c^e}\underline{\mathbf{t}}^m\cdot\tilde{\underline{\mathbf{u}}}^c dS - \int_{S_t^e}\bar{\mathbf{t}}\cdot\tilde{\mathbf{u}} dS - \int_{S_Q^e}\overline{Q}\tilde{\phi} dS \\ &- \int_{S_B^e}\overline{Q}_M\tilde{\psi} dS\Bigg\}\end{aligned} \tag{47}$$

If the grain contains no defects, basic solution set is to be used and all terms containing $\underline{\mathbf{u}}^c$ (u_i^c, φ^c, ψ^c) or $\mathbf{c}^c$ should be dropped from all previous equations, hence the second term in the stiffness matrix in eq. (45) is dropped and $\mathbf{K_{bvp}} = \mathbf{G}_{\mathbf{mq}}^T\mathbf{H}_{\mathbf{mm}}^{-1}\mathbf{G_{mq}}$ is used with no integrations done along $\partial\Omega_c^e$ in constructing $\mathbf{H_{mm}}$.

We denote this grain as "CPG-BVP" (or "CPG-BVPs" when using the impermeable void special solution set). This formulation clearly involves Lagrangian multipliers and hence suffers from LBB conditions (see Babuska, 1973; Brezzi, 1974), which are impossible to be satisfied a priori. This means that the eigenvalues of the stiffness matrix of an arbitrarily distorted grain, without a void or inclusion for instance, may include more than five zeros (for the three rigid-body and the two constant electric and magnetic potential modes) which indicates that the numerical formulation of the grain is not always stable. The stiffness matrix of CPG-BVP grain requires integration along the grain boundary to evaluate $\mathbf{G_{mq}}$ and $\mathbf{H_{mm}}$, and along the inclusion boundary to evaluate $\mathbf{G_{mc}}$, $\mathbf{H_{cc}}$ and $\mathbf{H_{mm}}$ as well as matrix inversions.

Note that the first eight Trefftz functions (corresponding to $n = 0$) should be eliminated from $\mathbf{N}^\alpha$ and $\mathbf{M}^\alpha$ when using this method because they correspond to rigid-body and constant potentials modes which do not contribute to the energy stored in the grain.

4.2. CPGs based on collocation method

In this method, the continuity between the matrix interior and boundary primal fields (mechanical displacements, electric and magnetic potentials) are enforced in a strong sense at several pre-selected collocation points $\mathbf{x}^{(r)}$, $r = 1, 2, \ldots R$ along the grain boundary $\partial\Omega^e$, and also when using the basic solution set (eqs. 23–25), the void/inclusion boundary conditions are enforced on a number of collocation points or curved segments ($\partial\Omega_c^e = \sum_{j=1}^{n_s}\partial\Omega_{cj}^e$) along the void/inclusion periphery. So we have:

1 Compatibility between matrix interior and boundary primal fields along $\partial\Omega^e$:

$$\underline{\mathbf{u}}^m\left(\mathbf{x}^{(r)},\mathbf{c}^m\right)=\underline{\tilde{\mathbf{u}}}\left(\mathbf{x}^{(r)},\mathbf{q}\right),\quad \mathbf{x}^{(r)}\in\partial\Omega^e\quad r=1,2,...R \tag{48}$$

2 Void boundary conditions: Traction-free and vanishing surface charge and magnetic flux densities conditions along $\partial\Omega_c^e$:

$$\int_{\partial\Omega_{cj}^e}\underline{\mathbf{t}}^m(\mathbf{x},\mathbf{c}^m)ds=0,\quad j=1,2,...n_s \tag{49}$$

or Inclusion boundary conditions: Traction reciprocity, continuities of electric charge and magnetic induction, and primal fields' continuity:

$$\begin{aligned}&\underline{\mathbf{t}}^m\left(\mathbf{x}^j,\mathbf{c}^m\right)+\underline{\mathbf{t}}^c\left(\mathbf{x}^j,\mathbf{c}^c\right)=0\quad \mathbf{x}^j\subset\partial\Omega_c^e,\quad j=1,2,...n_s\\&\underline{\mathbf{u}}^m\left(\mathbf{x}^j,\mathbf{c}^m\right)=\underline{\mathbf{u}}^c\left(\mathbf{x}^j,\mathbf{c}^c\right)\quad \mathbf{x}^j\subset\partial\Omega_c^e,\quad j=1,2,...n_s\end{aligned} \tag{50}$$

By selecting enough number of void/inclusion boundary segments or collocation points, and solving (48) and (49) or (50) in a least-square sense, $\mathbf{c}^m$ and $\mathbf{c}^c$ are related to $\mathbf{q}$ as follows:

$$\begin{bmatrix}\mathbf{A}_0 & 0\\ \mathbf{A}_2 & \mathbf{A}_3\end{bmatrix}\begin{Bmatrix}\mathbf{c}^m\\ \mathbf{c}^c\end{Bmatrix}=\begin{bmatrix}\mathbf{B}_0\\ 0\end{bmatrix}\mathbf{q} \tag{51}$$

This leads to:

$$\mathbf{c}^m=\mathbf{Z}^m\mathbf{q},\quad \mathbf{c}^c=\mathbf{Z}^c\mathbf{q} \tag{52}$$

Now, the interior fields are related to the nodal primal variables (step one), and the void/inclusion boundary conditions are enforced (step three), we just need to enforce the natural boundary conditions as well as the reciprocity conditions on the outer boundary (step two) using the following simple primitive field variational principle:

$$\begin{aligned}\Pi_2(u_i^m,\varphi^m,\psi^m)=\sum_{e=1}^{N}\Bigg\{&\int_{\partial\Omega^e}\frac{1}{2}(t_i^m u_i^m+Q^m\varphi^m+Q_M^m\psi^m)dS\\&-\int_{S_t^e}\bar{t}_i^m u_i^m dS-\int_{S_Q^e}\overline{Q}\varphi^m dS-\int_{S_B^e}\overline{Q}_M\psi^m dS\Bigg\}\end{aligned} \tag{53}$$

In matrix and vector notation Π_2 can be written as:

$$\begin{aligned}\Pi_2(\underline{\mathbf{u}}^m)=\sum_{e=1}^{N}\Bigg\{&\int_{\partial\Omega^e}\frac{1}{2}\underline{\mathbf{t}}^m\cdot\underline{\mathbf{u}}^m dS-\int_{S_t^e}\bar{\mathbf{t}}^m\cdot\mathbf{u}^m dS\\&-\int_{S_Q^e}\overline{Q}\varphi^m dS-\int_{S_B^e}\overline{Q}_M\psi^m dS\Bigg\}\end{aligned} \tag{54}$$

$$\begin{aligned}\Pi_2(\mathbf{q})=\sum_{e=1}^{N}\Bigg\{&\frac{1}{2}\mathbf{q}^T\mathbf{Z}^{mT}\left(\int_{\partial\Omega^e}\mathbf{M}^{mT}\underline{\mathbf{n}}^T\mathbf{N}^m dS\right)\mathbf{Z}^m\mathbf{q}\\&-\left[\int_{S_t^e}\bar{\mathbf{t}}^T\tilde{\mathbf{N}}_{\mathbf{u}}dS\quad\int_{S_Q^e}\overline{Q}\tilde{\mathbf{N}}_{\varphi}dS\quad\int_{S_B^e}\overline{Q}_M\tilde{\mathbf{N}}_{\psi}dS\right]\mathbf{q}\Bigg\}\\=\sum_{e=1}^{N}&\left\{\frac{1}{2}\mathbf{q}^T\mathbf{Z}^{mT}\mathbf{H}_{\mathbf{mm}}\mathbf{Z}^m\mathbf{q}-\mathbf{q}^T\mathbf{Q}\right\}\end{aligned} \tag{55}$$

where $\mathbf{H}_{\mathbf{mm}}=\int_{\partial\Omega^e}\mathbf{M}^{mT}\underline{\mathbf{n}}^T\mathbf{N}^m dS$ here. Setting the variation of Π_2 to zero gives:

$$\begin{aligned}\delta\Pi_2(\delta\mathbf{q})&=\sum_{e=1}^{N}\left\{\delta\mathbf{q}^T\left(\mathbf{Z}^{mT}\mathbf{H}_{\mathbf{mm}}\mathbf{Z}^m\right)\mathbf{q}-\delta\mathbf{q}^T\mathbf{Q}\right\}\\&=\sum_{e=1}^{N}\left\{\delta\mathbf{q}^T\mathbf{K}_{\mathbf{c}}\mathbf{q}-\delta\mathbf{q}^T\mathbf{Q}\right\}=0\end{aligned} \tag{56}$$

where $\mathbf{K}_{\mathbf{c}}=\mathbf{Z}^{mT}\mathbf{H}_{\mathbf{mm}}\mathbf{Z}^m$ is the stiffness matrix of "CPG-C" grain. This grain does not suffer from LBB conditions, because there is no Lagrangian multipliers involved. In order to obtain the stiffness matrix of this grain, only one matrix, $\mathbf{H}_{\mathbf{mm}}$, requires integration over the outer boundary, as well as the evaluation of $\mathbf{Z}^m$.

For an impermeable elliptical void, the special solution set (eq. (31)) can be used as an alternative to the collocation method to enforce the void boundary conditions. In this case, eq. (49) is not used in obtaining $\mathbf{c}^m$ in eqs. (51) and (52). The resulting grain is then denoted "CPG-Cs".

Collocation method can be replaced by the least squares method (which is equivalent to using infinite number of collocation points) generating "CPG-LS" and "CPG-LSs" grains. More details about this method can be found in (Bishay and Atluri, 2014).

4.3. On the selection of the maximum order of Trefftz functions

There are two conditions that should be considered in determining the maximum order of Trefftz functions, M, to be used in developing CPG grains. These two conditions are:

1 The number of Trefftz functions (or undetermined coefficients) m_T should be larger than the number of the grain's degrees of freedom (DOF) in order to ensure that the number of independent Trefftz modes are larger than or equal to the number of the grain's DOFs. Note that Lekhnitskii formulation (eqs. (23) and (24) or eq. (31)) generates some repeated modes. For example, and as mentioned earlier, the first eight Trefftz functions (corresponding to $n=0$) corresponds to the five rigid-body and constant potential modes. The number of degrees of freedom in any grain equals to the number of nodes $\times$ the number of degrees of freedom per node i.e. $4m$. Hence for rank sufficiency of the grain, the number of non-rigid-body Trefftz modes, $8M$ (or $16M$ when using the basic solution set for exterior domains), should be larger than the number of non-rigid-body degrees of freedom which is $4m-5$. This ensures that all grain types except CPG-BVP (or CPG-BVPs) are stable or rank sufficient. (It is impossible to ensure this for CPG-BVP grain because the grain formulation involves Lagrangian multipliers as mentioned earlier).
2 (Only for CPG-C grains) The number of equations used to solve for the undetermined coefficients should be larger than or equal to the number of these undetermined coefficients (m_T or

$m_T + m_{Tc}$ for the case of a grain with an inclusion). In developing CPG-C and CPG-Cs, we should select the number of collocation points used with any m-sided grain. Each collocation point provides four equations since we are collocating the four primal variables. If we use only two collocation points per edge then the total number of collocation equations in any m-sided polygonal grain is $m \times 2 \times 4 = 8m$. For CPG-C grains with voids where the basic solution set is to be used, $m_T = 8(2M + 1)$ because the negative exponents are also considered, thus increasing the number of unknowns; however $4n_s$ additional equations are added to enforce the void boundary condition on the void periphery. For CPG-C grains with inclusions, we have $m_T = 8(2M + 1)$ for the matrix and $m_{Tc} = 8(M_c + 1)$ for the inclusion, but we also have $4n_s$ additional equations that enforce the inclusion boundary conditions on the inclusion periphery. Here, we take $n_s = 48$ (where again n_s is the number of void/inclusion boundary segments).

So the conditions on the maximum order of Trefftz functions can be written as:

$$\begin{aligned}
&\frac{4m-5}{8} < M \le m-1 && \text{for CPG}-\text{Cs and CPG}-\text{C(with no void/inclusion)}\\
&\frac{4m-5}{16} < M \le \frac{2m+n_s-2}{4} && \text{for CPG}-\text{C(with void)}\\
&\frac{4m-5}{16} < M \le \frac{2m+n_s-4-2M_c}{4} && \text{for CPG}-\text{C(with inclusion)}
\end{aligned} \tag{57}$$

For CPG-Cs and CPG-C (with no void/inclusion), we can use $M = \lceil 4m - 5/8 \rceil$, where $\lceil . \rceil$ is a function that rounds a number up to an integer. This satisfies the two conditions. In this work we also use $M = \lceil 4m + 3/8 \rceil$ which is larger by one order. With CPG-C (with void or inclusion), larger values of M are to be used to increase the accuracy of the solution without violating the second condition.

Eq. (51) for CPG-C and CPG-Cs grains is over-constrained whenever the number of collocation points exceeds the number of undetermined coefficients, m_T. In addition, the system matrices in both CPG-C (eq. (51)) and CPG-LS are singular because of the repeated Trefftz functions. Hence in order to solve such systems, singular value decomposition (SVD) technique should be used. The SVD method can solve even the singular system of equations and produces the least squares solutions to the over-constrained systems.

4.4. Conditioning of the system matrices

The system of equations to be solved using any of the previous methods is ill-conditioned because of the exponential growth of the term Z_k^n as n is increased; hence we introduce a characteristic length to scale the Trefftz solution set.

For an arbitrary polygonal grain as shown in Fig. 1 (left), where the coordinate of the nodes are (x_1^j, x_3^j), $j = 1, 2, ..., m$, the center point of the polygon has coordinates (x_1^c, x_3^c). Relative to the local coordinates at the center point, we have $\widehat{z}_k = \widehat{x}_1 + \mu_k \widehat{x}_3 = (x_1 - x_1^c) + \mu_k (x_3 - x_3^c)$, k=1,2,3,4 and correspondingly, $\widehat{\xi}_k = \widehat{z}_k \pm \sqrt{\widehat{z}_k^2 - \left(a_o^2 + \mu_k^2 b_o^2\right)} \Big/ (a_o - i\mu_k b_o)$. Now, Z_k ($\widehat{z}_k$ for interior domains or $\widehat{\xi}_k$ for exterior domains) will be replaced by $\widehat{Z}_k / R_c$ where:

$$R_c = \max(R_{ck}), \quad R_{ck} = \max_j \sqrt{\left[\mathrm{Re}\left(\widehat{Z}_k^j\right)\right]^2 + \left[\mathrm{Im}\left(\widehat{Z}_k^j\right)\right]^2}, \quad j = 1, 2, ..., m \tag{58}$$

This is done only for terms with positive exponents. In this way, the exponential growth of Z_k^n is prevented as n increases because $0 < \left|(\widehat{Z}_k / R_c)^n\right| < 1$ for any point within the grain or along the grain boundaries.

5. Numerical examples

All grain types described above are programmed using MATLAB version R2014a in a 64-bit WINDOWS operating system, and executed on a PC computer equipped with Intel i7-2600K, 3.4 GHz CPU, and 8 GB RAM. In this section we give examples to show the capabilities of the proposed CPGs.

Simple problems that use grains with no voids, such as patch test and bending of a meso-scale piezoelectric or piezomagnetic panel, can be easily and accurately modeled using any grain type and any number of grains (with no voids) to mesh the problem domain, and the error in the whole structure is less than 1%.

5.1. Piezomagnetic domain with piezoelectric inclusion

Consider an infinite piezomagnetic domain with an elliptical piezoelectric inclusion subjected to vertical mechanical loading in the far field. For numerical implementations, the infinite domain is truncated into a rectangle with length L and width W. This can be modeled using only one CPG of piezomagnetic matrix with embedded piezoelectric inclusion. Both the poling direction of the piezoelectric phase and the magnetic bias direction (magnetic polarization) of the piezomagnetic phase are aligned with the global vertical axis. The piezomagnetic material is $CoFe_2O_4$ while the piezoelectric material is $BaTiO_3$. Properties of both materials can be found in (Lee et al., 2005) and plane strain assumption is used in this problem. Here we take $L = W = 1$ m, the volume fraction is 10%, b/a ratio is set to 0.8, the inclination angle is 0°, and the applied mechanical traction is $\sigma_o = 1$ GPa. Rollers are prescribed at the lower and left surfaces, while electric and magnetic grounds are prescribed at the lower left corner.

Figs. 4–7 show the distributions of electric and magnetic potentials, the two components of normal stress, the two components of electric displacement and the two components of magnetic induction around the inclusion.

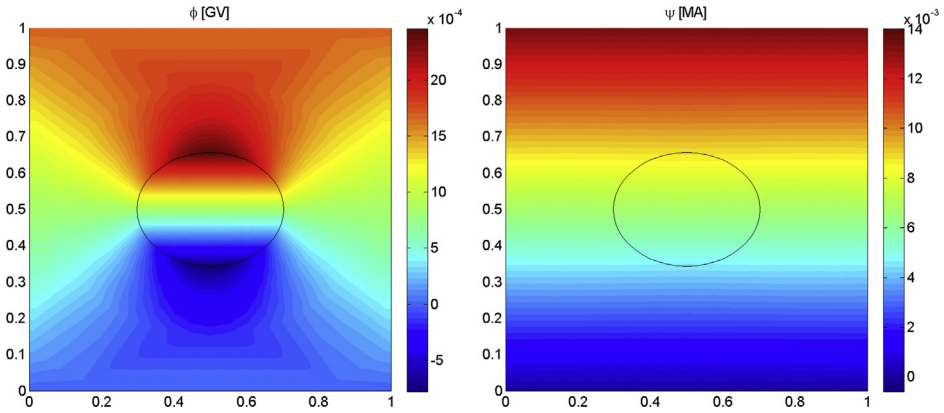

Fig. 4. Electric (left) and magnetic (right) potentials distributions.

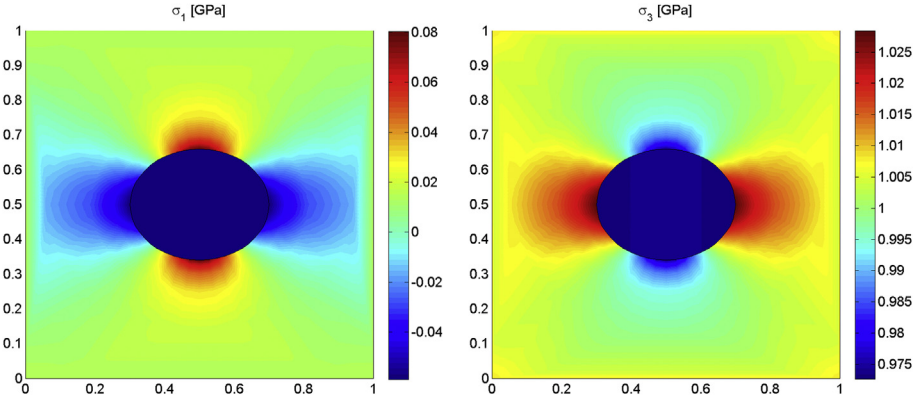

Fig. 5. σ_{11} (left) and σ_{33} (right) mechanical stress distributions.

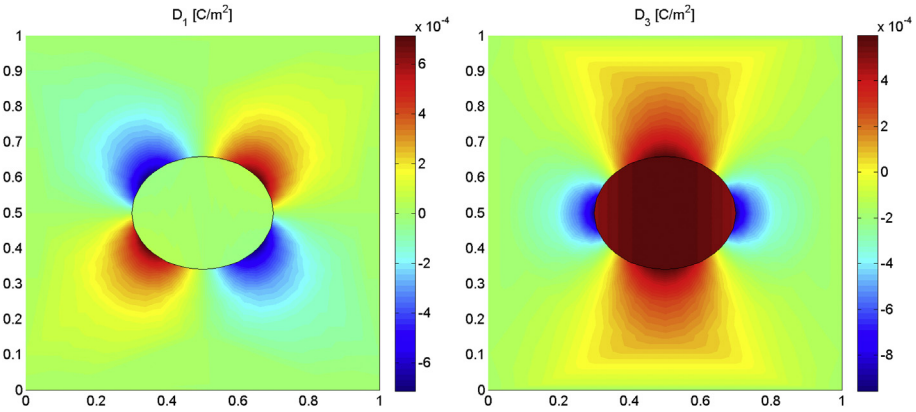

Fig. 6. Distributions of the components of electric displacement vector.

5.2. Evaluation of effective material properties of piezo-composite

In this subsection we determine the effective material properties of $BaTiO_3/CoFe_2O_4$ piezo-composite (Piezoelectric Barium Titanate particles embedded in Piezomagnetic Cobalt Ferrite matrix) as functions of the inclusions' volume fraction. Special computational models are used in evaluating the effective properties of this piezo-composite. Each of these special models ensures the presence of only one nonzero value in the magneto-electro-mechanical strain vector $[\varepsilon_{11} \quad \varepsilon_{33} \quad \varepsilon_{13} \quad -E_1 \quad -E_3 \quad -H_1 \quad -H_3]^T$. We then calculate the magneto-electro-mechanical stress vector $[\sigma_{11} \quad \sigma_{33} \quad \sigma_{13} \quad D_1 \quad D_3 \quad B_1 \quad B_3]^T$ on the four boundaries of the unit cell, and accordingly some material properties can be determined. For more details about these special models, readers are referred to (Bishay et al., 2014b) or (Lee et al., 2005). The unit cell can contain only one CPG or any number of CPGs. The results will change slightly every time we change the unit cell configuration (number and shapes of the grains). Both the magnetic bias direction in the piezomagnetic phase and the polarization in the piezoelectric phase are vertically upward.

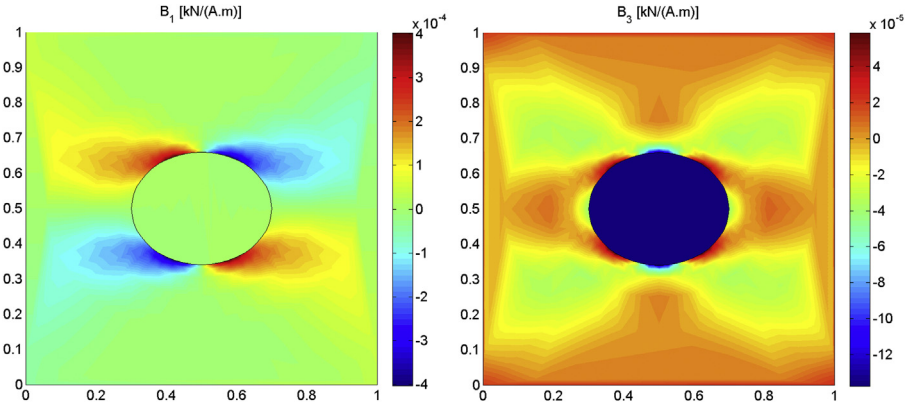

Fig. 7. Distributions of the components of magnetic induction.

Fig. 8 shows the predictions of effective material properties as functions of inclusions' volume fraction. The FEA results of Lee et al. (2005) are also shown for comparison. These results are also in excellent agreement with Mori-Tanaka's analytical model (Li and Dunn, 1998) as mentioned in (Lee et al., 2005). Very good agreement can be seen.

5.3. Modeling a piezo-composite microstructure

Consider a piezo-composite microstructure consisting of piezoelectric (PZT-4) spherical particles embedded in polymer matrix. The composite is subjected to tensile loading in the vertical direction of magnitude 1 GPa. During manufacturing some voids

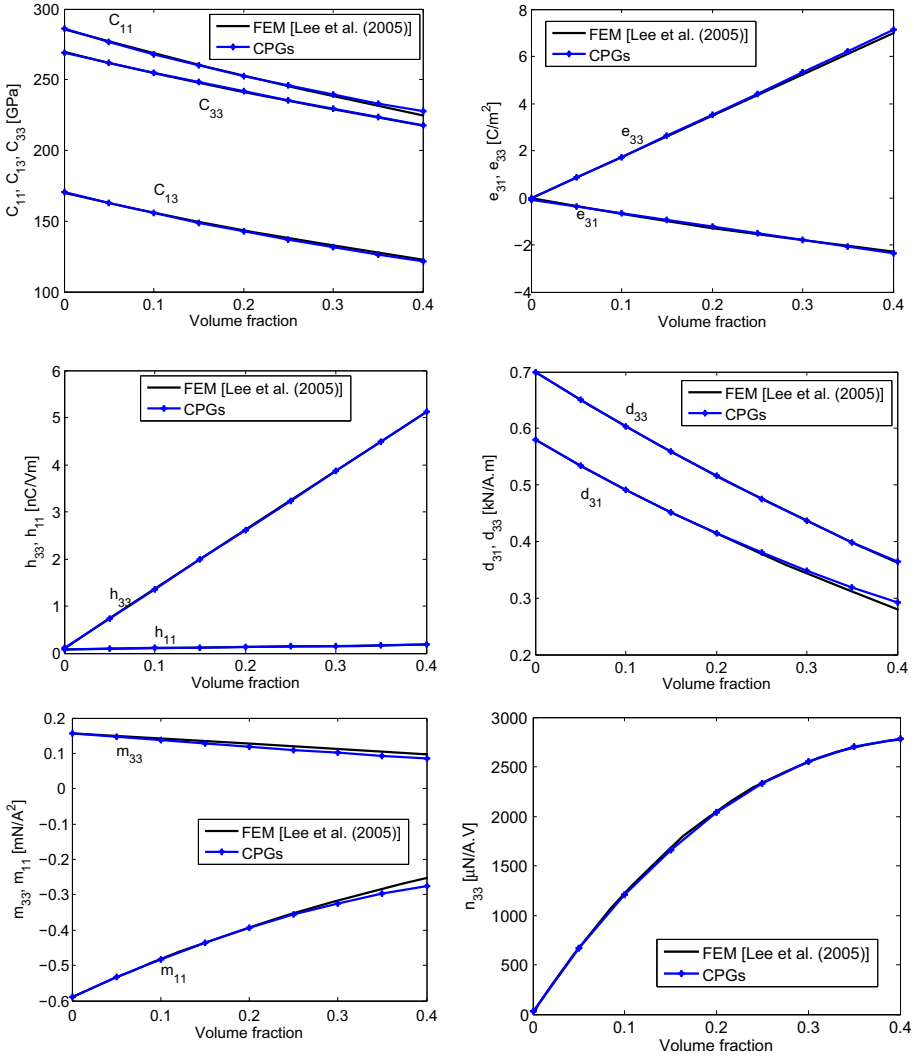

Fig. 8. Effective material properties of $BaTiO_3/CoFe_2O_4$ piezo-composite as functions of inclusions' volume fraction.

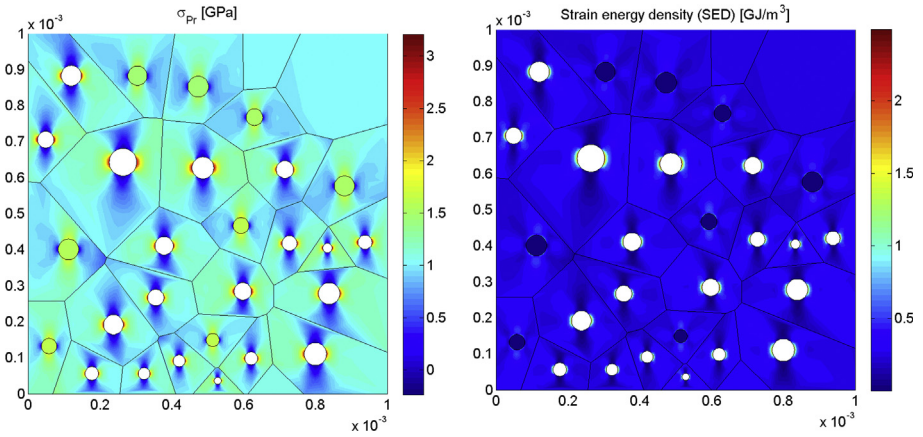

Fig. 9. Principal stress (left) and Strain energy density (right) distributions in the microstructure.

were nucleated in the microstructure. Considering that this microstructure consists of only 30 grains for illustration, we need only 30 CPGs to model it, while huge number of regular finite elements is required to get an acceptable accuracy. As the number of grains increases, the computational burden will highly increase in case of using finite element models, while with CPGs, the number of computational grains (super finite elements) is exactly the number of the modeled physical grains; thus saving a lot of computational effort, time and cost. In this model we create a random microstructure with 30 grains and we randomly distribute the grain types: some grains are solid, some contain voids and some contain inclusions. The dimensions of the domain are 1 mm × 1 mm. The material properties of PZT-4 are taken from (Sheng et al., 2006), while the polymer matrix has: $C_{11} = 3.86$, $C_{13} = 2.57$, $C_{55} = 0.64$ GPa, $h_{11} = h_{33} = 0.0796$ nC/(Vm)^2. Fig. 9 shows the principal stress and the strain energy density distribution plots. Locations of energy concentrations in the microstructure can be easily and accurately located.

6. Summary and conclusions

In this work, new multi-physics "super finite elements" are developed to model piezo-composites in the micro-scale. Each element (or computational grain) can have the shape of a material grain with embedded elliptical void or inclusion, and thus enable us to avoid excessively fine mesh around defects usually encountered with regular finite elements that can highly increase the model size especially with large number of defects. Piezoelectricity with magnetostatics or Piezomagnetism with electrostatics governing equations are solved in the domain of each element. Several types of such Computational-Piezo-Grains (CPGs) are presented based on boundary variational principle (BVP), collocation (C) or least squares (LS) methods. CPGs are successful in modeling piezo-composites with any number and distribution of voids or inclusions, and in estimating the effective material properties of piezoelectric-piezomagnetic composites.

Acknowledgment

This work was supported by a collaborative research agreement between the Army Research Lab's Vehicle Technology Division and University of California, Irvine. This support is gratefully acknowledged. The generous supports of Saint Martin's University, Lacey, WA, and California State University, Northridge to the first author are also thankfully acknowledged.

Appendix A

Three complex potential functions: Airy stress function, $\phi(x_1, x_3)$, electric scalar potential function, $\vartheta(x_1, x_3)$, and magnetic scalar potential function, $\rho(x_1, x_3)$, are introduced as:

$$\sigma_1 = \frac{\partial^2\phi(x_1,x_3)}{\partial x_3^2}, \quad \sigma_3 = \frac{\partial^2\phi(x_1,x_3)}{\partial x_1^2}, \quad \sigma_5 = -\frac{\partial^2\phi(x_1,x_3)}{\partial x_1\partial x_3},$$
$$D_1 = \frac{\partial\vartheta(x_1,x_3)}{\partial x_3}, \quad D_3 = -\frac{\partial\vartheta(x_1,x_3)}{\partial x_1}, \quad B_1 = \frac{\partial\rho(x_1,x_3)}{\partial x_3}, \quad B_3 = -\frac{\partial\rho(x_1,x_3)}{\partial x_1} \tag{A.1}$$

The balance rules for plane magneto-electro-elasticity (eq. (2)) in the absence of body force and free-charge density ($\overline{\mathbf{b}}_f = 0, \quad \overline{\rho_f} = 0$) are satisfied using eq. (A.1). By substituting eq. (A.1) into eq. (14) and invoking the following strain compatibility, Faraday's and Ampere's equations for 2D electrostatics and magnetostatics:

$$\frac{\partial^2\varepsilon_1}{\partial x_3^2} + \frac{\partial^2\varepsilon_3}{\partial x_1^2} - \frac{\partial^2\varepsilon_5}{\partial x_1\partial x_3} = 0, \quad \frac{\partial E_1}{\partial x_3} - \frac{\partial E_3}{\partial x_1} = 0, \quad \frac{\partial H_1}{\partial x_3} - \frac{\partial H_3}{\partial x_1} = 0 \tag{A.2}$$

Three differential equations coupled in $\phi(x_1, x_3)$, $\vartheta(x_1, x_3)$ and $\rho(x_1, x_3)$ can be obtained as:

$$\begin{aligned} &L_6\phi(x_1,x_3)-L_5\vartheta(x_1,x_3)-L_4\rho(x_1,x_3)=0,\\ &L_5\phi(x_1,x_3)+L_3\vartheta(x_1,x_3)+L_2\rho(x_1,x_3)=0,\\ &L_4\phi(x_1,x_3)+L_2\vartheta(x_1,x_3)+L_1\rho(x_1,x_3)=0 \end{aligned} \tag{A.3}$$

Where

$$L_1=\upsilon_{11}\frac{\partial^2}{\partial x_3^2}-2\upsilon_{13}\frac{\partial^2}{\partial x_1\partial x_3}+\upsilon_{33}\frac{\partial^2}{\partial x_1^2},\quad L_2=\kappa_{11}\frac{\partial^2}{\partial x_3^2}-2\kappa_{13}\frac{\partial^2}{\partial x_1\partial x_3}+\kappa_{33}\frac{\partial^2}{\partial x_1^2},$$

$$L_3=\beta_{11}\frac{\partial^2}{\partial x_3^2}-2\beta_{13}\frac{\partial^2}{\partial x_1\partial x_3}+\beta_{33}\frac{\partial^2}{\partial x_1^2},$$

$$L_4=-b_{11}\frac{\partial^3}{\partial x_3^3}+(b_{15}+b_{31})\frac{\partial^3}{\partial x_3^2\partial x_1}-(b_{13}+b_{35})\frac{\partial^3}{\partial x_3\partial x_1^2}+b_{33}\frac{\partial^3}{\partial x_1^3},$$

$$L_5=-g_{11}\frac{\partial^3}{\partial x_3^3}+(g_{15}+g_{31})\frac{\partial^3}{\partial x_3^2\partial x_1}-(g_{13}+g_{35})\frac{\partial^3}{\partial x_3\partial x_1^2}+g_{33}\frac{\partial^3}{\partial x_1^3},$$

$$L_6=S_{11}\frac{\partial^4}{\partial x_3^4}-2S_{15}\frac{\partial^4}{\partial x_3^3\partial x_1}+(2S_{13}+S_{55})\frac{\partial^4}{\partial x_3^2\partial x_1^2}-2S_{35}\frac{\partial^4}{\partial x_3\partial x_1^3}+S_{33}\frac{\partial^4}{\partial x_1^4}.$$

Eliminating $\vartheta(x_1, x_3)$ and $\rho(x_1, x_3)$ from eq. (A.3), the governing equations of plane magneto-electro-elasticity are reduced to the following eighth-order differential equation:

$$\left(L_1L_5^2-2L_2L_4L_5+L_1L_3L_6+L_3L_4^2-L_2^2L_6\right)\phi(x_1,x_3)=0 \tag{A.4}$$

If the material is piezoelectric ($\mathbf{b}=\boldsymbol{\kappa}=0$), then $L_2=L_4=0$, and eqs. (A.3) and (A.4) reduce to:

$$\left(L_5^2+L_3L_6\right)\phi(x_1,x_3)=0,\quad L_1\rho(x_1,x_3)=0 \tag{A.5}$$

if it is piezomagnetic ($\mathbf{g}=\boldsymbol{\kappa}=\mathbf{0}$), then $L_2=L_5=0$, and eqs. (A.3) and (A.4) take the form:

$$\left(L_4^2+L_1L_6\right)\phi(x_1,x_3)=0,\quad L_3\vartheta(x_1,x_3)=0, \tag{A.6}$$

while if it is only elastic dielectric ($\mathbf{g}=\mathbf{b}=\boldsymbol{\kappa}=\mathbf{0}$), then $L_2=L_4=L_5=0$, and eqs. (A.3) and (A.4) are reduced to:

$$L_6\phi(x_1,x_3)=0,\quad L_3\vartheta(x_1,x_3)=0,\quad L_1\rho(x_1,x_3)=0 \tag{A.7}$$

Eq. (A.5) for piezoelectric materials can be written symbolically as sixth and second degree differential equations for piezoelectricity and magnetostatics, respectively:

$$F_1F_2F_3F_5F_6F_7\phi(x_1,x_3)=0,\quad F_4F_8\rho(x_1,x_3)=0 \tag{A.8}$$

where $F_k=(\partial/\partial x_3)-\mu_k(\partial/\partial x_1)$ and $\mu_k(k=1,\ldots,8)$ are the roots of the characteristic eqs. (A.9) and (A.10). $\mu_1,\mu_2,\mu_3,\mu_5,\mu_6$ and μ_7 are obtained from the piezoelectricity eq. (A.9) while μ_4 and μ_8 are obtained from the magnetostatics eq. (A.10):

$$c_6\mu^6+c_5\mu^5+c_4\mu^4+c_3\mu^3+c_2\mu^2+c_1\mu+c_0=0. \tag{A.9}$$

$$\upsilon_{11}\mu^2-2\upsilon_{13}\mu+\upsilon_{33}=0 \tag{A.10}$$

where

$$\begin{aligned} &c_0=S_{33}\beta_{33}+g_{33}^2,\quad c_1=-2S_{35}\beta_{33}-2S_{33}\beta_{13}-2g_{33}(g_{13}+g_{35}),\\ &c_2=S_{33}\beta_{11}+4S_{35}\beta_{13}+\beta_{33}(2S_{13}+S_{55})+2g_{33}(g_{31}+g_{15})+(g_{13}+g_{35})^2,\\ &c_3=-2g_{11}g_{33}-2S_{15}\beta_{33}-2S_{35}\beta_{11}-2\beta_{13}(2S_{13}+S_{55})-2(g_{31}+g_{15})(g_{13}+g_{35}),\\ &c_4=S_{11}\beta_{33}+4S_{15}\beta_{13}+\beta_{11}(2S_{13}+S_{55})+2g_{11}(g_{13}+g_{35})+(g_{31}+g_{15})^2,\\ &c_5=-2S_{11}\beta_{13}-2S_{15}\beta_{11}-2g_{11}(g_{31}+g_{15}),\quad c_6=S_{11}\beta_{11}+g_{11}^2. \end{aligned}$$

Eq. (A.6) for piezomagnetic materials can be written symbolically as sixth and second degree differential equations for piezomagnetism and electrostatics, respectively:

$$F_1F_2F_4F_5F_6F_8\phi(x_1,x_3)=0,\quad F_3F_7\vartheta(x_1,x_3)=0 \tag{A.11}$$

where μ_k are the roots of the characteristic eqs. (A.12) and (A.13). $\mu_1,\mu_2,\mu_4,\mu_5,\mu_6$ and μ_8 are obtained from the piezomagnetism eq. (A.12) while μ_3 and μ_7 are obtained from the electrostatics eq. (A.13):

$$d_6\mu^6+d_5\mu^5+d_4\mu^4+d_3\mu^3+d_2\mu^2+d_1\mu+d_0=0. \tag{A.12}$$

$$\beta_{11}\mu^2-2\beta_{13}\mu+\beta_{33}=0 \tag{A.13}$$

where

$$d_0 = S_{33}\upsilon_{33} + b_{33}^2, \quad d_1 = -2S_{35}\upsilon_{33} - 2S_{33}\upsilon_{13} - 2b_{33}(b_{13} + b_{35}),$$
$$d_2 = S_{33}\upsilon_{11} + 4S_{35}\upsilon_{13} + \upsilon_{33}(2S_{13} + S_{55}) + 2b_{33}(b_{31} + b_{15}) + (b_{13} + b_{35})^2,$$
$$d_3 = -2b_{11}b_{33} - 2S_{15}\upsilon_{33} - 2S_{35}\upsilon_{11} - 2\upsilon_{13}(2S_{13} + S_{55}) - 2(b_{31} + b_{15})(b_{13} + b_{35}),$$
$$d_4 = S_{11}\upsilon_{33} + 4S_{15}\upsilon_{13} + \upsilon_{11}(2S_{13} + S_{55}) + 2b_{11}(b_{13} + b_{35}) + (b_{31} + b_{15})^2,$$
$$d_5 = -2S_{11}\upsilon_{13} - 2S_{15}\upsilon_{11} - 2b_{11}(b_{31} + b_{15}), \quad d_6 = S_{11}\upsilon_{11} + b_{11}^2.$$

Eq. (A.7) for elastic dielectric materials can be written symbolically as forth degree differential equation for elasticity and two second degree differential equations for electrostatics and magnetostatics:

$$F_1F_2F_5F_6\phi(x_1,x_3) = 0, \quad F_3F_7\vartheta(x_1,x_3) = 0, \quad F_4F_8\rho(x_1,x_3) = 0 \tag{A.14}$$

where μ_k are the roots of the characteristic eqs. (A.15), (A.13) and (A.10). μ_1, μ_2, μ_5 and μ_6 are obtained from the elasticity eq. (A.15), μ_3 and μ_7 are obtained from the electrostatics eq. (A.13), while μ_4 and μ_8 are obtained from the magnetostatics eq. (A.10):

$$S_{11}\mu^4 - 2S_{15}\mu^3 + (2S_{13} + S_{55})\mu^2 - 2S_{35}\mu^3 + S_{33} = 0 \tag{A.15}$$

Note that if there are no piezoelectric and piezomagnetic couplings, eqs. (A.9) and (A.12) break down, and eqs. (A.15), (A.13) and (A.10) should be used to obtain the roots μ_k.

In general, the roots of eqs. (A.9) and (A.10) for piezoelectric materials, (A.12) and (A.13) for piezomagnetic materials, or those of eqs. (A.15), (A.13) and (A.10) for elastic dielectric materials are complex with four conjugate pairs:

$$\mu_1 = A_{\mu1} + iB_{\mu1}, \quad \mu_2 = A_{\mu2} + iB_{\mu2}, \quad \mu_3 = A_{\mu3} + iB_{\mu3},$$
$$\mu_4 = A_{\mu4} + iB_{\mu4},$$
$$\mu_5 = \overline{\mu}_1, \quad \mu_6 = \overline{\mu}_2, \quad \mu_7 = \overline{\mu}_3, \quad \mu_8 = \overline{\mu}_4 \tag{A.16}$$

in which $i = \sqrt{-1}$, $A_{\mu k}$ and $B_{\mu k}$ $(k = 1, 2, 3, 4)$ are all distinct. Over-bar denotes complex conjugate.

Integration of eq. (A.8) leads to the general solution for the complex potential functions $\phi(x_1, x_3)$ and $\rho(x_1, x_3)$ for piezoelectric materials as:

$$\phi(x_1,x_3) = 2\mathrm{Re}\sum_{k=1}^{3}\phi_k(z_k), \quad \rho(x_1,x_3) = 2\mathrm{Re}(\omega_4(z_4)) \tag{A.17}$$

where $\phi_k(z_k)$ is an arbitrary function of the complex variable $z_k = x_1 + \mu_k x_3$, and $\omega_4(z_4)$ is an arbitrary function of the complex variable $z_4 = x_1 + \mu_4 x_3$. By virtue of eqs. (A.3) and (A.17), the general solution for the complex potential function $\vartheta(x_1, x_3)$ can be expressed as:

$$\vartheta(x_1,x_3) = 2\mathrm{Re}\sum_{k=1}^{3}\eta_k\frac{\partial\phi_k(z_k)}{\partial z_k} \tag{A.18}$$

Where

$$\eta_k = -\frac{l_2(\mu_k)}{l_1(\mu_k)}, \quad l_1(\mu_k) = \beta_{11}\mu_k^2 - 2\beta_{13}\mu_k + \beta_{33},$$
$$l_2(\mu_k) = -g_{11}\mu_k^3 + (g_{15} + g_{31})\mu_k^2 - (g_{13} + g_{35})\mu_k + g_{33}.$$

Integration of eq. (A.11) leads to the general solution for the complex potential functions $\phi(x_1, x_3)$ and $\vartheta(x_1,x_3)$ for piezomagnetic materials as:

$$\phi(x_1,x_3) = 2\mathrm{Re}\sum_{k=1,2,4}\phi_k(z_k), \quad \vartheta(x_1,x_3) = 2\mathrm{Re}(\omega_3(z_3)) \tag{A.19}$$

By virtue of eqs. (A.3) and (A.19), the general solution for the complex potential function $\rho(x_1, x_3)$ can be expressed as:

$$\rho(x_1,x_3) = 2\mathrm{Re}\sum_{k=1,2,4}\tau_k\frac{\partial\phi_k(z_k)}{\partial z_k} \tag{A.20}$$

Where

$$\tau_k = -\frac{l_4(\mu_k)}{l_3(\mu_k)}, \quad l_3(\mu_k) = \upsilon_{11}\mu_k^2 - 2\upsilon_{13}\mu_k + \upsilon_{33},$$
$$l_4(\mu_k) = -b_{11}\mu_k^3 + (b_{15} + b_{31})\mu_k^2 - (b_{13} + b_{35})\mu_k + b_{33}.$$

Integration of eq. (A.14) leads to the general solution for the complex potential functions $\phi(x_1, x_3)$, $\vartheta(x_1,x_3)$ and $\rho(x_1, x_3)$ for elastic dielectric materials as:

$$\phi(x_1,x_3) = 2\mathrm{Re}\sum_{k=1}^{2}\phi_k(z_k); \quad \vartheta(x_1,x_3) = 2\mathrm{Re}(\omega_3(z_3));$$
$$\rho(x_1,x_3) = 2\mathrm{Re}(\omega_4(z_4)) \tag{A.21}$$

Introducing new complex potential functions:

$$\omega_k(z_k) = \frac{\partial\phi_k(z_k)}{\partial z_k} \tag{A.22}$$

where $k = 1,2,3$ for the piezoelectric case ($\omega_4(z_4)$ is already defined in eq. (A.17) for this case), $k = 1,2,4$ for the piezomagnetic case ($\omega_3(z_3)$ is already defined in eq. (A.19) for this case), and $k = 1,2$ for the mechanical part of the uncoupled material ($\omega_3(z_3)$ and $\omega_4(z_4)$ are already defined in eq. (A.21) for this case), the expressions of $\phi(x_1, x_3)$, $\vartheta(x_1,x_3)$ and $\rho(x_1, x_3)$ in eq. (A.17)–(A.21) can be generalized to account for all cases as:

$$\phi(x_1,x_3)=2\mathrm{Re}\sum_{k=1}^{4}\gamma_k\phi_k(z_k),\quad \vartheta(x_1,x_3)=2\mathrm{Re}\sum_{k=1}^{4}\lambda_k\omega_k(z_k),$$
$$\rho(x_1,x_3)=2\mathrm{Re}\sum_{k=1}^{4}\Delta_k\omega_k(z_k) \tag{A.23}$$

where for uncoupled (elastic dielectric) materials: $\gamma_k=\delta_{k1}+\delta_{k2},\quad \lambda_k=\delta_{k3},\quad \Delta_k=\delta_{k4},$
for piezoelectric: $\gamma_k=1-\delta_{k4},\quad \Delta_k=\delta_{k4},$

$$\lambda_k=\gamma_k\eta_k=(1-\delta_{k4})\frac{g_{11}\mu_k^3-(g_{15}+g_{31})\mu_k^2+(g_{13}+g_{35})\mu_k-g_{33}}{\beta_{11}\mu_k^2-2\beta_{13}\mu_k+\beta_{33}}$$

and for piezomagnetic: $\gamma_k=1-\delta_{k3},\quad \lambda_k=\delta_{k3},$

$$\Delta_k=\gamma_k\tau_k=(1-\delta_{k3})\frac{b_{11}\mu_k^3-(b_{15}+b_{31})\mu_k^2+(b_{13}+b_{35})\mu_k-b_{33}}{\upsilon_{11}\mu_k^2-2\upsilon_{13}\mu_k+\upsilon_{33}}$$

δ_{ij} is the Kronecker delta. Substituting eq. (A.23) into eq. (A.1), general expressions for the stress, electric displacement, magnetic induction, strain, electric field and magnetic field components for any type of material can be obtained in terms of the complex potential functions $\omega_k(z_k)$ as in eq. (18), where:

$$p_k=\gamma_k\left(S_{11}\mu_k^2+S_{13}-S_{15}\mu_k\right)+\lambda_k(g_{11}\mu_k-g_{31})+\Delta_k(b_{11}\mu_k-b_{31}),$$
$$q_k=\gamma_k\left(S_{13}\mu_k^2+S_{33}-S_{35}\mu_k\right)+\lambda_k(g_{13}\mu_k-g_{33})+\Delta_k(b_{13}\mu_k-b_{33}),$$
$$r_k=\gamma_k\left(S_{15}\mu_k^2+S_{35}-S_{55}\mu_k\right)+\lambda_k(g_{15}\mu_k-g_{35})+\Delta_k(b_{15}\mu_k-b_{35}),$$
$$s_k=\gamma_k\left(g_{11}\mu_k^2+g_{13}-g_{15}\mu_k\right)-\lambda_k(\beta_{11}\mu_k-\beta_{13}),\quad t_k=\gamma_k\left(g_{31}\mu_k^2+g_{33}-g_{35}\mu_k\right)-\lambda_k(\beta_{13}\mu_k-\beta_{33}),$$
$$h_k=\gamma_k\left(b_{11}\mu_k^2+b_{13}-b_{15}\mu_k\right)-\Delta_k(\upsilon_{11}\mu_k-\upsilon_{13}),\quad l_k=\gamma_k\left(b_{31}\mu_k^2+b_{33}-b_{35}\mu_k\right)-\Delta_k(\upsilon_{13}\mu_k-\upsilon_{33}).$$

The roots $\mu_k(k=1,\ldots,8)$ depend on the material type as described above. Note that if there are no piezoelectric and piezomagnetic couplings, eqs. (A.9) and (A.12) break down, and eqs. (A.15), (A.13) and (A.10) should be used to obtain the roots μ_k.

Invoking the gradient relations in eq. (3), the general solution for displacement, electric and magnetic potentials can be obtained as in eq. (17).

References

Babuska, I., 1973. The finite element method with Lagrangian multipliers. Numer. Math. 20 (3), 179–192.

Bishay, P.L., Atluri, S.N., 2012. High-performance 3D hybrid/mixed, and simple 3D Voronoi cell finite elements, for macro- & micro-mechanical modeling of solids, without using multi-field variational principles. CMES: Comput. Model. Eng. Sci. 84 (1), 41–98.

Bishay, P.L., Atluri, S.N., 2013. 2D and 3D multiphysics Voronoi cells, based on radial basis functions, for direct mesoscale numerical simulation (DMNS) of the switching phenomena in ferroelectric polycrystalline materials. CMC: Comput. Model. Eng. Sci. 33 (1), 19–62.

Bishay, P.L., Atluri, S.N., 2014. Trefftz-Lekhnitskii grains (TLGs) for efficient direct numerical simulation (DNS) of the micro/meso mechanics of porous piezoelectric materials. Comput. Mater. Sci. 83, 235–249.

Bishay, P.L., Alotaibi, A., Atluri, S.N., 2014a. Multi-region Trefftz collocation grains (MTCGs) for modeling piezoelectric composites and porous materials in direct and inverse problems. J. Mech. Mater. Struct. 9 (3).

Bishay, P.L., Dong, L., Atluri, S.N., 2014b. Multi-physics computational grains (MPCGs) for direct numerical simulation (DNS) of piezoelectric composite/porous materials and structures. Comput. Mech. 54 (5), 1129–1139.

Blackburn, J.F., Vopsaroiu, M., Cain, M.G., 2008. Verified finite element simulation of multiferroic structures solutions for conducting and insulating systems. J. Appl. Phys. 104 (7), 074104.

Brezzi, F., 1974. On the existence, uniqueness and approximation of saddle-point problems arising from Lagrangian multipliers. Rev. Française D'automatique, Inform. Rech. Opérationnelle, Anal. Numérique 8 (2), 129–151.

Cao, C., Yu, A., Qin, Q.H., 2013. A new hybrid finite element approach for plane piezoelectricity with defects. Acta Mech. 224, 41–61.

Cheong, S., Mostovoy, M., 2007. Multiferroics: a magnetic twist for ferroelectricity. Nat. Mater. 6, 13–20.

Cullity, B.D., 1971. Fundamentals of magnetostriction. J. Metals 1, 323.

Domingues, J.S., Portela, A., Castro, P.M.S.T., 1999. Trefftz boundary element method applied to fracture mechanics. Eng. Fract. Mech. 64, 67–86.

Dong, L., Atluri, S.N., 2013. SGBEM Voronoi Cells (SVCs), with embedded arbitrary-shaped inclusions, voids, and/or cracks, for micromechanical modeling of heterogeneous materials. CMC: Comput. Mater. Continua 33 (2), 111–154.

Dong, L., Atluri, S.N., 2012a. A simple multi-source-point Trefftz method for solving direct/inverse SHM problems of plane elasticity in arbitrary multiply-connected domains. CMES: Comput. Model. Eng. Sci. 85 (1), 1–43.

Dong, L., Atluri, S.N., 2012b. T-Trefftz Voronoi cell finite elements with elastic/rigid inclusions or voids for micromechanical analysis of composite and porous materials. CMES: Comput. Model. Eng. Sci. 83 (2), 183–219.

Dong, L., Atluri, S.N., 2012c. Development of 3D T-Trefftz Voronoi cell finite elements with/without spherical voids &/or Elastic/Rigid inclusions for micromechanical modeling of heterogeneous materials. CMC: Comput. Mater. Continua 29 (2), 169–211.

Dong, L., Atluri, S.N., 2012d. Development of 3D Trefftz Voronoi cells with Ellipsoidal voids &/or elastic/rigid inclusions for micromechanical modeling of heterogeneous materials. CMC: Comput. Mater. Continua 30 (1), 39–82.

Dong, L., Atluri, S.N., 2012e. SGBEM (Using non-hyper-singular traction BIE), and super elements, for non-collinear fatigue-growth analyses of cracks in stiffened panels with composite-patch repairs. CMES: Comput. Model. Eng. Sci. 89 (5), 417–458.

Ghosh, S., 2011. Micromechanical Analysis and Multi-scale Modeling Using the Voronoi Cell Finite Element Method. CRC Press/Taylor & Francis.

IEEE Std 319-1990, 1991. IEEE Standard on Magnetostrictive Materials.

Jayabal, K., Menzel, A., 2011. On the application of the polygonal finite element method for two-dimensional mechanical and electromechanically coupled problems. Comput. Model. Eng. Sci. 73 (2), 183–207.

Jayabal, K., Menzel, A., 2012a. Polygonal finite elements for three-dimensional Voronoi-cell-based discretisations. Eur. J. Comput. Mech. 21 (1–2), 92–102.

Jayabal, K., Menzel, A., 2012b. Voronoi-based three-dimensional polygonal finite elements for electromechanical problems. Comput. Mater. Sci. 64, 66–70.

Kamentsev, K.E., Fetisov, Y.K., Srinivasan, G., 2006. Low-frequency nonlinear magnetoelectric effects in a ferrite-piezoelectric multilayer. Appl. Phys. Lett. 89 (14), 142510–142510-3.

Laletsin, U., Padubnaya, N., Srinivasan, G., Devreugd, C.P., 2004. Frequency dependence of magnetoelectric interactions in layered structures of ferromagnetic alloys and piezoelectric oxides. Appl. Phys. A: Mater. Sci. Process 78, 33–36.

Lee, J., Boyd IV, J.G., Lagoudas, D.C., 2005. Effective properties of three-phase electro-magneto-elastic composites. Int. J. Eng. Sci. 43, 790–825.

Lekhnitskii, S.G., 1968. Anisotropic Plates. Gordon and Breach, Science Publishers, New York.

Lekhnitskii, S.G., 1981. Theory of Elasticity of an Anisotropic Body. Mir Publishers, Moscow.

Li, J.Y., Dunn, M.L., 1998. Micromechanics of magnetoelectroelastic composite materials: average fields and effective behavior. J. Intell. Mater. Syst. Struct. 9, 404–416.

McCaig, M., 1977. Permanent Magnets in Theory and Practice. Pentech Press. ISBN 0-7273-1604-4.

Nan, C.W., Cai, N., Liu, L., Zhai, J., Ye, Y., Lin, Y.H., 2003. Coupled magnetic–electric properties and critical behavior in multiferroic particulate composites. J. Appl. Phys. 94, 5930.

Nan, C.-W., Bichurin, M.I., Dong, S., Viehland, D., Srinivasan, G., 2008. Multiferroic magnetoelectric composites: historical perspective, status, and future directions. J. Appl. Phys. 103, 031101.

Petrov, V.M., Srinivasan, G., Laletsin, V., Bichurin, M.I., 2007. Half-metallic ferromagnetism in zinc-blende CaC, SrC, and BaC from first principles. Phys. Rev. B 75, 174442.
Pian, T.H.H., 1964. Derivation of element stiffness matrices by assumed stress distribution. Am. Inst. Aeronaut. Astronaut. 2, 1333–1336.
Piltner, R., 1985. Special finite elements with holes and internal cracks. Int. J. Num. Methods Eng. 21, 1471–1485.
Ryu, J., Priya, S., Uchino, K., Kim, H.E., 2002. Magnetoelectric effect in composites of magnetostrictive and piezoelectric materials. J. Electroceramics 8, 107–119.
Sheng, N., Sze, K.Y., Cheung, Y.K., 2006. Trefftz solutions for piezoelectricity by Lekhnitskii's formalism and boundary collocation method. Int. J. Numer. Methods Eng. 65, 2113–2138.
Sze, K.Y., Sheng, N., 2005. Polygonal finite element method for nonlinear constitutive modeling of polycrystalline ferroelectrics. Finite Elem. Anal. Des. 42, 107–129.
Wang, H., Qin, Q.H., 2012. A new special element for stress concentration analysis of a plate with elliptical holes. Acta Mech. 223, 1323–1340.
Wang, X.W., Zhou, Y., Zhou, W.L., 2004. A novel hybrid finite element with a hole for analysis of plane piezoelectric medium with defects. Int. J. Solids Struct. 41, 7111–7128.
Xu, X.L., Rajapakse, R.K.N.D., 1998. Boundary element analysis of piezoelectric solids with defects. Compos. B 29 (5), 655–669.
Xu, X.L., Rajapakse, R.K.N.D., 1999. Analytical solution for an arbitrarily oriented void/crack and fracture of piezoceramics. Acta Mater. 47, 1735–1747.
Zhai, J., Cai, N., Shi, Z., Lin, Y., Nan, C.-W., 2004. Magnetic-dielectric properties of NiFe2O4/PZT particulate composites. J. Phys. D. 37, 823–827.
Zhang, J., Katsube, N., 1997. A polygonal element approach to random heterogeneous media with rigid ellipses or elliptic voids. Comput. Methods Appl. Mech. Engrg. 148, 225–234.